UNIVERSITAT POLITÈCNICA DE VALÈNCIA

ETSI Aeroespacial y Diseño Industrial

UNIVERSITAT POLITÈCNICA DE VALÈNCIA

School of Aerospace Engineering and Industrial Design

Comparative study of numerical solvers for noise propagation of UAVs in urban environments

End of Degree Project

Bachelor's Degree in Aerospace Engineering

AUTHOR: Noguerón Moya, Ignacio

Tutor: García Tíscar, Jorge

ACADEMIC YEAR: 2023/2024

Abstract

Due to the increasingly faster developments on UAVs, and an ever-growing demand of online shopping, it is to be expected that suppliers will start using automated drones to deliver their products. However, this creates a need for new legislation, not only because of safety concerns, but also due to an increase in noise pollution. The level of noise produced by a great number of UAVs flying at low altitudes is not negligible, hence the necessity of predicting which flight paths and operating conditions would minimize the noise emitted. Besides, numerical models need to be efficient, given that it should be possible to simulate whole cities in a timely manner, so that companies can perform their own studies to determine routes for maximizing benefits while still complying with regulations. At the other side of the spectrum, researchers need more accurate models to develop methods to improve the noise absorption of façades, streets, etc.

This work aims to explain the bases of noise modelling, as well as to compare solvers with varying degrees of precision and efficiency. A simple case study of a UAV, modelled as a spherical source with directivity, hovering over a set of buildings with simple geometries has been used as a benchmark.

Keywords: UAV, drone, noise propagation, numerical solver, urban noise, simulation

Resumen

Debido a los desarrollos cada vez más rápidos en los UAV, y una demanda creciente en la compra de productos en línea, cabe esperar que los proveedores comiencen a utilizar drones automatizados para realizar las entregas de productos. Sin embargo, esto genera la necesidad de nueva legislación, no sólo por motivos de seguridad, sino también debido al incremento en la contaminación acústica. El nivel de ruido producido por un gran número de UAV volando a altitudes bajas no es despreciable, por ello la necesidad de predecir las rutas de vuelo y condiciones de operación que minimizarían la emisión de ruido. Además, los modelos numéricos necesitan ser eficientes, dado que debería ser posible simular ciudades enteras en marcos de tiempo razonables, para que las empresas puedan realizar sus propios estudios que les permitan determinar rutas de entrega que maximicen los beneficios ateniéndose a las regulaciones. En el otro lado del espectro, los investigadores necesitan modelos más precisos para desarrollar métodos para mejorar la absorción de ruido de fachadas, calles, etc.

Este trabajo pretende explicar las bases del modelado de la propagación de ruido, además de comparar *software* con diversos grados de precisión y eficiencia. Un caso de estudio simple de un UAV, modelado como una fuente esférica con directividad, volando a punto fijo sobre un conjunto de edificios con geometrías simples se ha utilizado como referencia para realizar la comparativa.

Palabras clave: UAV, dron, propagación de ruido, *solver* numérico, ruido urbano, simulación

Resum

A causa dels desenvolupaments cada vegada més ràpids en els UAV, i una demanda creixent en la compra de productes en línia, cal esperar que els proveïdors comencen a utilitzar drons automatitzats per a realitzar els lliuraments de productes. Tanmateix, això genera la necessitat de nova legislació, no sols per motius de seguretat, sinó també a causa de l'increment en la contaminació acústica. El nivell de soroll produït per un gran nombre de UAV volant a altituds baixes no és menyspreable, per això la necessitat de predir les rutes de vol i condicions d'operació que minimitzarien l'emissió de soroll. A més, els models numèrics necessiten ser eficients, atés que hauria de ser possible simular ciutats senceres en marcs de temps raonables, perquè les empreses puguen realitzar els seus propis estudis que els permeten determinar rutes de lliurament que maximitzen els beneficis atenint-se a les regulacions. En l'altre costat de l'espectre, els investigadors necessiten models més precisos per a desenvolupar mètodes per a millorar l'absorció de soroll de façanes, carrers, etc.

Este treball pretén explicar les bases del modelatge de la propagació de soroll, a més de comparar programari amb diversos graus de precisió i eficiència. Un cas d'estudi simple d'un UAV, modelat com una font esfèrica amb directivitat, volant a punt fix sobre un conjunt d'edificis amb geometries simples s'ha utilitzat com a referència per a realitzar la comparativa.

Paraules clau: UAV, dron, propagació de soroll, *solver* numèric, soroll urbà, simulació

Agradecimientos

Quiero, en primer lugar, agredecer a mi madre su apoyo incondicional desde que tengo memoria, sin el que seguramente no me encontraría donde estoy en este momento. Si he podido tener la suerte de estudiar lo que me gusta, es por ella.

Agradecer también a mis amigos Olga, Quique y Juan haber sido mis compañeros a lo largo de este periplo de cuatro años, que desde luego no hubiera sido lo que ha sido sin ellos. Si he disfrutado como lo he hecho de ir a clase ha sido por vosotros.

Por último, agradecer la ayuda de Federico Nahuel Ramírez, cuyo apoyo ha sido crucial para la realización de este Trabajo de Fin de Grado.

Contents

Figures iii

Tables v

1. Introduction 1

    1.1. Objectives 2

2. Theoretical Background 3

    2.1. Wave-based methods 3

    2.2. Geometrical Acoustics: Gaussian Beam Tracing 6

    2.3. Geometrical Acoustics: CNOSSOS-EU 11

3. State of the Art 16

4. Methodology 21

    4.1. Available software 21

    4.2. Set up of the openCFS simulations 24

    4.3. Set up of the NoiseModelling simulations 30

5. Results 35

    5.1. openCFS 35

        5.1.1. Frequency-domain simulations 35

        5.1.2. Time-domain simulations 37

    5.2. NoiseModelling 42

6. Conclusions 48

    6.1. Future work 48

References 50

Appendix A: Project's Budget 55

    A.1. Tasks performed by personnel involved 55

    A.2. Resources employed 55

    A.3. Costs 56

        A.3.1. Personnel 56

        A.3.2. Software 57

A.3.3. Equipment 57
A.3.4. Total costs 58
Appendix B: Bid specifications 59
B.1. Workplace specifications 59
B.1.1. General safety specifications 59
B.1.2. Order, cleanliness and maintenance 60
B.1.3. Ambient specifications 60
B.1.4. Workplace lighting 60
B.1.5. Restrooms and resting places 61
B.1.6. First aid equipment and facilities 61
B.2. Technical specifications 61
B.2.1. Hardware specifications 61
B.2.2. Software specifications 62
Appendix C: Relationship of the thesis with the Sustainable Development Goals 63

Figures

Figure 2.1. Concept of a wavefront. Points belonging to the same wavefront receive the same waveform simultaneously [23]. 7
Figure 2.2. Ray-centred coordinates of a point R' in the vicinity of a central ray [25]..... 9
Figure 2.3. Calculation of the path difference in homogeneous conditions. 14
Figure 2.4. Calculation of the path difference in favourable conditions. 14
Figure 3.1. Geometry and regions of the FDTD-PE simulation [12]. 17
Figure 4.1. Geometry for the openCFS simulation. 25
Figure 4.2. Geometry defined in Gmsh. Surfaces must have 4 boundaries to produce a transfinite structured mesh. 27
Figure 4.3. Mesh for frequency-domain simulations produced by Gmsh. 28
Figure 4.4. Simulated and fitted directivities of the acoustic pressure of a XOAR PJN 9X7" propeller at the BPF and first harmonic when rotating with angular frequency of 7375 rpm. 29
Figure 4.5. Comparison between satellite image and the OpenStreetMap database geometry (Benidorm). 31
Figure 4.6. Position of the UAV point source in the NoiseModelling simulation domain... 33
Figure 4.7. NoiseModelling's Web Page Services Graphic User Interface. 34
Figure 5.1. SPL field produced by the BPF and its first harmonic. 36
Figure 5.2. Amplitude of the acoustic pressure along the façades of the centre building ... 36
Figure 5.3. Snapshots of the time-domain simulation of the base case. 38
Figure 5.4. Comparison of acoustic pressure field between time-domain and frequency-domain simulations. 39
Figure 5.5. Time-domain simulation with only reflecting ground. 39
Figure 5.6. Time-domain simulation with no reflecting boundaries. 40
Figure 5.7. Comparison of acoustic pressure at the bottom-centre of the street canyons... 41
Figure 5.8. Comparison of transient SPL at the bottom-centre of the street canyons. 42

Figure 5.9. Noise map produced with diffraction and reflections of order 3. 43
Figure 5.10. Noise maps produced with diffraction, and with reflections of order 1 (left) and 2 (right). 43
Figure 5.11. Close-up of the noise maps produced with diffraction, and with reflections of order 1 (left) and 2 (right). 44
Figure 5.12. Noise maps produced by first order reflections and with (left) and without (right) modelling diffraction. 45
Figure 5.13. Detail of the noise maps produced by first order reflections and with (left) and without (right) modelling diffraction. 45
Figure 5.14. Comparison of noise maps produced when the maximum source-reflection distance is set to 50 (left) and 800 m (right). 46
Figure 5.15. Close-up of the comparison of noise maps produced when the maximum source-reflection distance is set to 50 (left) and 800 m (right). 47

Tables

Table 4.1. Summary of sound propagation methods used by software and the phenomena they can simulate. 23
Table 4.2. Summary of user-friendliness features of reviewed solvers. 24
Table 4.3. Geometry of the openCFS simulations. 25
Table 4.4. Air properties at sea level and 20 °C. 28
Table 4.5. Attributes of the UAV point source. 32
Table A.1. Resources employed in the project's elaboration. 56
Table A.2. Gross personnel costs. 57
Table A.3. Software costs. 57
Table A.4. Gross total cost of the project. 58
Table A.5. Final cost of the whole project. 58
Table B.1. Specifications of personal laptop. 61
Table C.1. Relationship of the thesis with the Sustainable Development Goals. 63

1. Introduction

The advances in aeronautical technology have caused UAVs (Unmanned Aerospace Vehicles), also referred as "drones", to become a candidate for civil uses, e.g., surveillance or transport of both goods and even people. Given the increase on the demand of online shopping, companies like Amazon or DHL have already started to develop drones, and literature suggests that there is a market to exploit [1], even if it is only a viable option in some countries [2]. Even if UAVs could be expected to coexist with ground vehicles [3], the apparition of drones in the urban airspace is sure to be noticed by the population. According to surveys conducted by Airbus [4], as well as other researchers [5], [6], the main concern of the public is safety, followed by noise. It is to be considered that, even if smaller drones like the ones being currently developed by Amazon do not produce much noise, Airbus is more interested in the market of UAMs (Urban Air Mobility) to transport people in crowded cities, which are much larger and therefore produce much more noise. In any case, if the predictions of backyard delivery's demand are correct, a large amount of small UAV's is to be expected, which can also produce large amounts of noise.

Noise pollution is a problem for both the human population and the animal welfare; hence the airspace should be regulated in this regard. In order to properly determine operation routes, no-fly zones, etc., mathematical models need to be used to assess the noise produced by the UAVs during operation. However, modelling noise propagation accurately in order to obtain meaningful data is a complex task, due to the amount of elements that have a relevant impact on the SPL (Sound Pressure Level) [7]. The acoustic pressure propagation is highly dependent on the geometry and topology of cities, as reflections on the façades and other surfaces are a dominant factor when source and receiver are far from each other, or they have no direct line-of-sight. The acoustic properties of the surfaces, mainly the ground, also cause scattering, which is crucial in less populated areas. Dense vegetation also has to be considered, as it absorbs and scatters sound. Wind profiles and other meteorological effects also influence noise propagation, especially over rooftops, which, given the scope of this project, is of special interest. If all these effects are to be computed in a realistic manner, that is to say, that the models used compute all these physical phenomena, the computational cost becomes really high even for small domains. Besides, including the absorption and scattering of surfaces requires previous experiments to gather data for all the frequency spectrum of interest, as the complex impedance of a surface depends on frequency.

On another note, the source has also to be modelled, as the sound produced by UAVs is highly directional, and the frequencies at which it emits noise depend on its rpm and number of blades per rotor. Henceforth it is necessary to extract experimental data in a controlled environment (an anechoic chamber) or to simulate the UAV through numerical models.

Apart from predicting the SPL, it should be considered that not all noises are equally perceived, and the higher pitches produced by UAVs during operation are more annoying than those lower pitches produced by road vehicles [8]. The noise produced by UAVs is also perceived significantly more annoying when it is listened in rural and suburban environments, whereas in highly populated zones the noise is masked by that of traffic [9]. There exists no direct way of assessing how a noise will be perceived, hence the need for auralization of noise and surveys.

This field of study has not yet been fully developed, so there are not yet available open-source codes that have been consolidated as standards for either research or engineering calculations. It has to be considered that, in a near future UAV's traffic will have to be regulated, software should be able to calculate with adequate accuracy large domains with multiple moving sources within reasonable timeframes. In the next sections of this work, a review of the alternatives being currently developed by researchers will be presented, and some of the available software will be used to demonstrate their capabilities and limitations.

1.1. Objectives

Considering the above information, this thesis aims to:

1. Provide an easy but thorough background to the sound propagation models that are currently being used by researchers, so that becomes possible to follow papers on the matter.
2. Give context on what are researchers currently working on, the many complexities and limiting factors that arise from the problem of sound propagation numerical modelling, and the possible future breakthroughs.
3. Review available software to carry out simulations, exposing their strengths and weaknesses.
4. Perform simulations in some of these software to explain in detail how do they work and provide examples of problems that can be solved by them.

2. Theoretical Background

There are two main approaches regarding the computation of acoustics: on the one hand, there are the methods based on the wave equations, that predict accurately the pressure waves phenomena (if data used is actually representative of the real case) by solving the physics behind the problem; on the other hand, GA (geometrical acoustics), also commonly referred as engineering methods, compute the sound perceived by a "receiver" by computing rays between the source of the sound and the receiver. As the name would suggest, GA is commonly less precise but also much faster and less computationally demanding. In both cases, there exist multitude of methods with varying degrees of precision and efficiency.

2.1. Wave-based methods

Although acoustic formulation in inhomogeneous moving and multiphase media exist [10], most solvers consider the air to behave as a monophasic gas. If the meteorological effects are to be considered, the physical equations that describe the acoustic waves are the following:

$$\left(\frac{\partial}{\partial t} + \mathbf{u}\cdot\nabla\right)\mathbf{u_a} + (\mathbf{u_a}\cdot\nabla)\mathbf{u} + \frac{1}{\rho}\nabla p_a = \frac{\mathbf{F}}{\rho} \tag{1}$$

$$\left(\frac{\partial}{\partial t} + \mathbf{u}\cdot\nabla\right)p_a + \rho c^2\nabla\cdot\mathbf{u_a} = \rho c^2 Q \tag{2}$$

where $\mathbf{u} = \mathbf{u}(\mathbf{x}, t)$ is the wind or average speed, $\mathbf{u_a} = \mathbf{u_a}(\mathbf{x}, t)$ is the acoustic speed, $p_a = p_a(\mathbf{x}, t)$ is the acoustic pressure, $c = c(\mathbf{x}, t)$ is the speed of sound, $\rho = \rho(\mathbf{x}, t)$ is the density of air, and $\mathbf{F} = \mathbf{F}(\mathbf{x}, t)$ and $Q = Q(\mathbf{x}, t)$ are external forces and a source term respectively. All quantities are expressed in SI units.

Note that Equations (1) and (2) are coupled and contain both spatial and time derivatives of the variables of interest. This causes the PDE system to be computationally demanding in most cases. Furthermore, mesh needs to be highly refined over all the domain: 10 samples are necessary per wavelength in order to maintain errors low, hence all the mesh needs to have a cell size such that the highest frequency of interest is computed correctly [11], [12], [13], [14]. In contrast, as it will be discussed later, GA solve first order differential equations that only depend on time.

It should be considered that, these equations come from the full set of fluid dynamic equations, linearised and particularized for the specific case of atmospheric air and acoustic

waves (terms that produce gravitational waves have been neglected in this formulation). For a more detailed analysis of the scope of these equations and other more complex models, as well as mathematical demonstrations, it is highly encouraged to check references [10], [15]. Equations (1) and (2) have been widely used for FDTD (Finite-Difference Time-Domain) simulations and are the basis for all wave-based numerical methods. The two coupled equations can be further simplified and reduced to a single equation if the meteorological effects are not relevant to the simulation, e.g., sound propagating between buildings:

$$\left(\frac{1}{c^2}\frac{\partial^2}{\partial t^2} - \Delta\right) p_a = 0 \tag{3}$$

Note that in Equation (3), it has also been assumed that $c \approx$ const. and that there are no forces or sources to take into account.

In order to use Equations (1) and (2) in a simulation, one must know beforehand the ambient values of c, ρ and $\mathbf{u}$. The two former quantities can be easily obtained from a model of the atmosphere, while the latter one can be defined through wind profiles, usually obtained by performing a CFD simulation, or experimental data. In addition to that, boundary conditions must be defined for all surfaces limiting the domain. The boundary conditions can be defined in terms of pressure (Dirichlet), known as sound soft; normal velocity or acceleration (Neumann), known as sound hard; or impedance, normally expressed as complex and frequency-dependant. Numerous models have been proposed for complex impedances. As an example, the Delany-Bazley-Miki model has been widely used due to its validity in all the f/σ_0 range [16], [17]:

$$Z_c = \rho_0 c_0 \left[1 + 5.50\left(10^3 \frac{f}{\sigma_0}\right)^{-0.632} - j8.43\left(10^3 \frac{f}{\sigma_0}\right)^{-0.632}\right] \tag{4}$$

where ρ_0 and c_0 are the respective properties of air, σ_0 is the static air flow resistivity of the material in kPa s m^{-2}, and f is the frequency in Hz.

Sound soft BCs are normally only used for liquid-gas interfaces; hence they are out of the scope of this work. On the contrary, sound hard BCs are equivalent to infinitely high impedance surfaces, and are used frequently to model materials like concrete, thus avoiding obtaining a model of the complex impedance. There is another kind of BC that is key when studying external acoustics, i.e., when it is necessary to model an open or infinite domain.

Due to the discretization of the domain, if no action is taken, even if a surface has no reflective BC, numerical reflections appear causing unphysical and spurious phenomena in FDTD; and in the case of FEM, not specifying a BC is actually equivalent to having a completely reflective surface. This problem is solved by adding a new absorbing region to the domain referred as Perfectly Matched Layer (PML), in which the wave equations are modified to act unphysically and have a damping independently of frequency and angle of incidence. The PML was first formulated by Berenger when dealing with this same problem when simulating electro-magnetic waves through FDTD [18], and later formulated and validated by Yuan for acoustic simulations [19]. Nowadays, PMLs are the standard for open domain problems for both FDTD and FEM simulations, though they are not formulated equally. Conceptually, the absorption of the impinging waves is achieved by using complex values for the speed of sound (c_c) and density (ρ_c) so that the region impedance is a perfect match with that of the propagation region:

$$Z = \rho_c c_c = \rho c \tag{5}$$

The PML is actually achieved by performing a complex change of the spatial variables [20]:

$$\zeta \to \tilde{\zeta} = \int_0^{\zeta} s_\zeta(\zeta')\ \mathrm{d}\zeta' \tag{6}$$

where $\zeta = x, y, z$ and s_ζ is the complex co-ordinate stretching variable. In order to have a perfect match between the regions, $s_\zeta = 1$ at the boundary of the PML and the propagation region, and must have an increasing imaginary part (damping component) as it propagates through the PML. In order to obtain the Berenger's formulation of the PML,

$$s_\zeta = 1 + j\frac{\sigma_\zeta(\zeta)}{\omega} \tag{7}$$

where $\sigma_\zeta(\zeta)$ is the damping function and ω is the angular frequency of the wave, which has a value of 0 in the boundary and increases monotonically in the PML.

Even though, theoretically, the change of variables should produce a continuous function, it has been proven that the inverse distance absorbing function

$$\sigma_\zeta(\zeta) = \frac{c}{L - \zeta} \tag{8}$$

in which L is the thickness of the PML, as can be seen, is not equal to 0 at the boundary of both regions, and yet, produces an optimal reduction of the reflections due to producing

an unbounded integral in the change of variables that causes an infinitely large damping [21]. As it will be discussed in later sections, this is the PML model used by open-source software OpenCFS.

Readers may have noticed that impedance and PML boundary conditions have been defined in the frequency domain instead of the time domain (used in FDTD). This means that Equations from (4) to (8) have to be converted to the frequency domain through a Fast Fourier Transform (FFT) in order to be implemented. Alternatively, FEM solvers can also be expressed in the frequency domain if the problem is periodic. This also drastically reduces computation times, as the time dependence of the problem can be eliminated from the problem if expressed with complex variables. However, that means that it is not possible to have moving sources or receivers in the latter case.

Though more limited in various regards, frequency-based methods are still used nowadays in some applications. It allows to highly simplify the system of PDEs to solve, as time dependence is eliminated. The most popular methods used in the frequency domain are the Fast-Field Program (FFP), which consists in wavenumber integration through a FFT, and the Parabolic Equation (PE), which significantly simplifies the Helmholtz equation resulting from applying a Fourier transform to Equations (1) and (2) by only considering reflections and scattering in directions close to the propagation one. Wavenumber integration and PE solvers are both usually formulated for one-way wave propagation, so they are usually not suitable for urban scenarios, where reflections that affect the SPL close to the source location are to be expected [10]. Still, as it will be discussed later, some studies have managed to implement these frequency-domain methods for urban acoustics [12], [22].

2.2. Geometrical Acoustics: Gaussian Beam Tracing

It is considered that acoustic waves have a wavefront that travels with speed c with respect to the ambient medium (see Figure 2.1.). This wavefront is approximately plain in the vicinity of any point contained by it, i.e., its surface is continuous and differentiable. The last statement will be relevant later, as it will be necessary to express equations in a 2D reference system perpendicular to the propagation direction contained in the vicinity of a point of the wavefront.

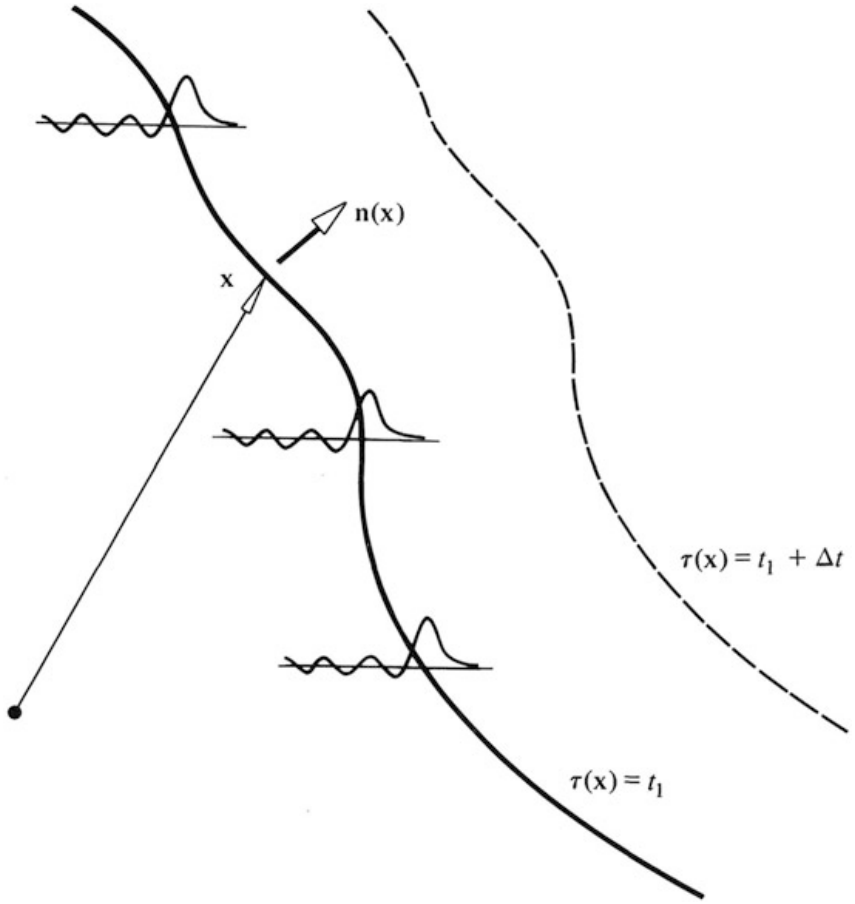

Figure 2.1. Concept of a wavefront. Points belonging to the same wavefront receive the same waveform simultaneously [23].

It is possible then to describe the position of a moving point P that lies at the wavefront $t = \tau(\mathbf{x})$ with the following equation:

$$\frac{d\mathbf{x}_P}{dt} = \mathbf{u}(\mathbf{x}_P, t) + \mathbf{n}(\mathbf{x}_P, t)c(\mathbf{x}_P, t) \tag{9}$$

where $\mathbf{n}(\mathbf{x}_P, t)$ is the unitary vector normal to the wavefront at point P. Without further assumptions, it is possible to reach the following system of first order differential equations in cartesian coordinates [23]:

$$\frac{dx_i}{dt} = \frac{c^2 s_i}{\Omega} + u_i \tag{10}$$

$$\frac{ds_i}{dt} = -\frac{\Omega}{c}\frac{\partial c}{\partial x_i} - \sum_{j=1}^{3} s_j \frac{\partial u_j}{\partial x_i} \tag{11}$$

where the vector $\mathbf{s}$ is the "wave-slowness", defined as $\mathbf{s} = \nabla\tau(\mathbf{x})$, therefore parallel to $\mathbf{n}$; and the parameter Ω is defined as $\Omega = 1 - \mathbf{u} \cdot \mathbf{s}$. The name "wave-slowness" comes from the fact that the reciprocal of $|\mathbf{s}|$ is $c + \mathbf{n} \cdot \mathbf{u}$, which is the speed with which the wavefront moves normal to itself.

Note that Equations (10) and (11) are of first order and decoupled, making them easily solvable with any method of numerical integration. Furthermore, besides the sound speed and wind velocity ambient fields, only the initial conditions of the wavefront are necessary. That is what makes GA much more efficient than wave-based methods. However, these equations only describe the path of a single ray. Depending on how the solver is completed, it is referred to as a ray-tracing method or as a Gaussian Beam Tracing (GBT) method. Conceptually, the difference between them is if all of the energy is concentrated into the main ray, or if the main ray is associated with a beam with a gaussian profile. GBT is the most promising method on acoustic problems due to normal ray-tracing producing perfect shadows and singularities at caustics (points where rays from the same wavefront intersect) [24].

After calculating the central rays, gaussian beams are constructed around them. In order to do so, a new ray-centred system of coordinates has to be defined, as shown in Figure 2.2. As the "wave-slowness" is perpendicular to the wavefront, it can be used to define the vectors $\mathbf{e_1}$ and $\mathbf{e_2}$, perpendicular between them, referred to as polarization vectors, that form the wavefront plane at the vicinity of the central ray [25]. Additionally, variable r corresponds to the arclength travelled along the central ray:

$$\mathbf{e_1} = \begin{bmatrix} e_{1x} \\ e_{1y} \\ e_{1z} \end{bmatrix} = \begin{bmatrix} \dfrac{cs_1s_3\cos\phi + s_2\sin\phi}{L} \\ \dfrac{cs_2s_3\cos\phi - s_1\sin\phi}{L} \\ cL\cos\phi \end{bmatrix}, \mathbf{e_2} = \begin{bmatrix} e_{2x} \\ e_{2y} \\ e_{2z} \end{bmatrix} = \begin{bmatrix} \dfrac{cs_1s_3\cos\phi - s_2\sin\phi}{L} \\ \dfrac{cs_2s_3\cos\phi + s_1\sin\phi}{L} \\ -cL\cos\phi \end{bmatrix} \tag{12}$$

where $L = \sqrt{s_1^2 + s_2^2}$ and ϕ is the rotation angle, given by:

$$\frac{d\phi}{dr} = \frac{s_3\left(s_2\dfrac{\partial c}{\partial x} - s_1\dfrac{\partial c}{\partial y}\right)}{L^2c(r)} \tag{13}$$

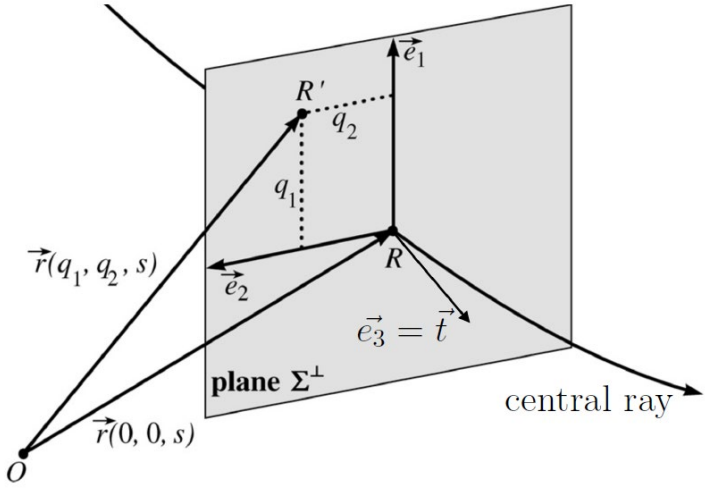

Figure 2.2. Ray-centred coordinates of a point $\boldsymbol{R}'$ in the vicinity of a central ray [25].

By integrating Equation (13) along the ray, it is possible to obtain the polarization vectors at any given point of the ray through Equation (12) without the need to compute curvature and torsion. The position of an arbitrary point may be expressed as:

$$\mathbf{x}_{P'}(r) = \mathbf{x}_P(r) + q_1(r)\mathbf{e_1}(r) + q_2(r)\mathbf{e_2}(r) \tag{14}$$

where q_1, q_2 are the coordinates of the new defined system of reference.

The spreading and phase-front change of the beam are given by [26]:

$$\frac{dp_i}{dr} = \frac{1}{c^2} c_{i,j} q_i, \quad i,j = 1,2 \tag{15}$$

$$\frac{dq_i}{dr} = cp_i \tag{16}$$

where p_1, p_2 are the components of the slowness vector in the wavefront reference system, and $c_{i,j}$ is the matrix of second derivatives of sound speed:

$$c_{i,j} = \begin{bmatrix} \dfrac{\partial^2 c(r)}{\partial q_1^2} & \dfrac{\partial^2 c(r)}{\partial q_1 \partial q_2} \\ \dfrac{\partial^2 c(r)}{\partial q_2 \partial q_1} & \dfrac{\partial^2 c(r)}{\partial q_2^2} \end{bmatrix} \tag{17}$$

In order to construct the gaussian beam in a 3D environment, Equations (15) and (16) have to be solved for two linearly independent solutions [25], [27]:

$$\mathbf{P}(r) = \begin{bmatrix} p_1^I & p_1^{II} \\ p_2^I & p_2^{II} \end{bmatrix}, \mathbf{Q}(r) = \begin{bmatrix} q_1^I & q_1^{II} \\ q_2^I & q_2^{II} \end{bmatrix} \tag{18}$$

For a point source, these matrices have initial values [25]:

$$\mathbf{P}(r_0) = \begin{bmatrix} 1 & 0 \\ 0 & 1 \end{bmatrix}, \mathbf{Q}(r_0) = \begin{bmatrix} 0 & 0 \\ 0 & 0 \end{bmatrix} \tag{19}$$

Finally, the beam energy at the receptor is computed as:

$$u_{beam}(q_1, q_2, r) = \frac{A(r)}{\sqrt{|\mathbf{Q}|}} e^{i\omega \left| t(r) + \frac{1}{2}\mathbf{q}^T(r)\mathbf{P}(r)\mathbf{Q}^{-1}(r)\mathbf{q}(r) \right|} \tag{20}$$

where $A(r)$ is the amplitude of the wave at arclength r of the central ray and $t(r)$ is the elapsed time between the point source and the receiver.

To calculate the total energy received at a receiver, first all rays that pass near the point of interest are identified, and afterwards the total effect of all of them is added. This would also be the case with standard ray-tracing, but the energy of the central ray would be considered. The benefit of the GBT method is that once the rays of interest have been identified, the spreading from the central ray to the receiver is taken into account, producing smoother shadows with less ray calculations.

In the case of ray-tracing/GBT, there is no need for PMLs. Reflections are usually modelled through image sources (the angle of incidence is equal to the angle of reflection). Refraction is also easily implemented through new initial values of matrices $\mathbf{P}$ and $\mathbf{Q}$, applied once the interface between to media is reached [26]. Impedance is usually approximated through an absorption coefficient α such that the energy of the reflected rays is $(1 - \alpha)$ times the one of the incident rays. GA make actually easier to simulate scattering, a phenomenon caused by the irregularities of the surfaces in which due to multiple close reflections in small cavities rays can propagate in seemingly random directions after being reflected. However, special efforts have to be made in order to model diffraction, by creating different ray-propagating models. Also, especially in the case of external acoustics, a large number of rays have to be computed in order to reach with a considerable amount of them to all the desired receivers, as a lot of the energy is lost just by exiting the domain.

The GA methods are also limited by being inherently limited to high frequencies. This is because low frequencies can cause resonances, although this concern is more relevant in room acoustics, where the Schröder frequency, i.e., the cross-over frequency from which resonances do not appear, is much higher. Still, resonances can take place in street canyons, so data should be reviewed with scepticism when low frequencies are being calculated (normally below 100 – 200 Hz). The Schröder frequency [28] is given by:

$$f_c = 2000\sqrt{\frac{T_{60}}{V}} \tag{23}$$

where T_{60} is the 60 dB reverberation time in seconds and V the volume of the enclosure in cubic meters.

Another limitation of GA is cases with complex geometries and topographies were a high number of reflections and diffractions are to be expected. This is because, due to memory constraints, ray paths usually have to be limited to a given number of reflections (each time a reflection takes place, a new ray has to be created; even more if scattering is included in the model).

2.3. Geometrical Acoustics: CNOSSOS-EU

With the aim of having common criteria for evaluation of environmental noise in all the European Union, the Common Noise Assessment Methods, known as CNOSSOS-EU, were established through the Commission Directive 2015/996 of 19 May 2015 [29]. The CNOSSOS-EU numerical model is split into two branches: on the one hand, it includes models to simulate the emission produced by road traffic, rail traffic, industrial buildings and aircraft close to airports; on the other hand, there is a highly efficient propagation numerical model, which allows to simulate whole cities in a timely manner. As there is yet to be included an emission model for UAV's traffic, in this work, only the sound propagation model is of interest. Luckily, the CNOSSOS-EU method allows to incorporate any point-source by means of specifying the values of SPL at different frequencies, even specifying directivity.

The CNOSSOS-EU path finding method is based on the image source model, in which the paths between a source S and a receiver R are split into straight segments, and reflections are modelled through image sources S', so that the angle of incidence and reflection coincide. The CNOSSOS-EU model only considers reflections on vertical surfaces and applies a correction for the effect of ground. This makes this method not suitable to calculate noise above buildings if the source is also above them, as no reflections with rooftops are considered. Nevertheless, it is still valid if the receivers are located below at a height lower than all rooftops.

The path finding algorithm used by CNOSSOS-EU forms propagation paths along vertical planes. The path is form by segments between the source and the receiver (S, R), between the source and a diffraction point (S, O), between two diffraction points (O, O'), or between a diffraction point and the receiver (O, R). Heights of both ends of a segment

are needed to later compute the ground effect correction. These are computed with respect to a mean plane, obtained through least squares: the topography used by CNOSSOS-EU is formed by polygons, so the ground contained in the vertical plane of the path can be expressed as a polyline.

The calculation process is split into two: calculation of the attenuation in favourable conditions and in homogeneous conditions. Then both results are weighted to obtain the 'long-term' sound level. This is made to take into account the influence of meteorology in the calculations, as different conditions (upwind path, downwind path, temperature gradients…) produce different results. Instead of defining a specific meteorological condition, the sound levels are weighted by the mean occurrence p of favourable conditions in the direction of the path:

$$L_{LT} = 10 \log_{10} \left(p \cdot 10^{\frac{L_F}{10}} + (1-p) \cdot \ 10^{\frac{L_H}{10}} \right) \tag{22}$$

where variable L is the SPL in dB, and suffixes LT, F and H mean 'long-term', 'favourable' and 'homogeneous' respectively.

Regarding the calculation of the SPL, it is computed in frequency bands. Starting with the source's SPL, a series of attenuation corrections are applied:

$$L_F = L_{W,0,dir} - A_F, \qquad L_H = L_{W,0,dir} - A_H \tag{23}$$

$$A_F = A_{div} + A_{atm} + A_{boundary,F}, \qquad A_H = A_{div} + A_{atm} + A_{boundary,H} \tag{24}$$

Note that between favourable and homogenous conditions, only the term related to boundaries, $A_{boundary}$, is different. The attenuation terms are respectively related to geometrical divergence, atmospheric absorption, and ground effect and diffractions.

The first term, geometrical divergence, is simply computed from the direct 3D slant d between the source and the receiver:

$$A_{div} = 20 \log_{10}(d) + 11 \tag{25}$$

The atmospheric absorption is also obtained from distance d:

$$A_{atm} = \alpha_{atm} \frac{d}{1000} \tag{26}$$

where α_{atm} is the atmospheric attenuation coefficient in dB/km at the nominal centre frequency for each frequency band, in accordance with ISO 9613-1. These coefficients are giv-

en for a temperature of 15 °C, a relative humidity of 70% and an atmospheric pressure of 101 325 Pa.

Lastly, the ground effect and diffractions are grouped in the same term. The ground effect is computed based on dimensionless coefficients G, with values in a scale from 0 to 1, in which 0 means totally reflective and 1 is totally absorptive. The G values are mainly linked to ground's porosity. This coefficient is the same for all frequencies, unlike in the real scenario. A path is assigned a G value through a weighted mean:

$$G_{path} = \frac{\sum_{i=1}^{n} G_i d_i}{\sum_{i=1}^{n} d_i} \tag{27}$$

The process to calculate the attenuation caused by the ground involves multiple equations for both homogeneous and favourable conditions and for cases with and without diffraction, and is out of the scope of this work. Still, the complete method is available at [29]. The important thing is that all calculations can be computed easily through arithmetic formulas, making it very efficient.

Regarding the calculation of the attenuation produced by diffraction, it requires first to determine the path difference between the direct path between S and R and the trajectory considering all diffractions. It is at this stage that the method is different for homogeneous and favourable conditions. In homogeneous conditions, all paths are considered to be formed by straight segments, as can be seen in Figure 2.3., whereas in favourable conditions, all segments share a radius of curvature Γ, as shown in Figure 2.4. The value of Γ is given by:

$$\Gamma = \max(1000,8d) \tag{28}$$

and the length of a curved trajectory between points M and N, noted as $\widehat{MN}$, is easily obtained from:

$$\widehat{MN} = 2\Gamma \arcsin\left(\frac{MN}{2\Gamma}\right) \tag{29}$$

In homogeneous conditions, if the receiver R is not masked by any obstacles, the path difference is calculated in the same way, but the sign is negative. In favourable conditions, an auxiliary point A, placed at the intersection of the straight sound ray SR and the extension of the diffracted obstacle is used. In this case, the path difference is given by:

$$\delta_F = 2\hat{SA} + 2\hat{AR} - \hat{SO} - \hat{OR} - \hat{SR} \tag{30}$$

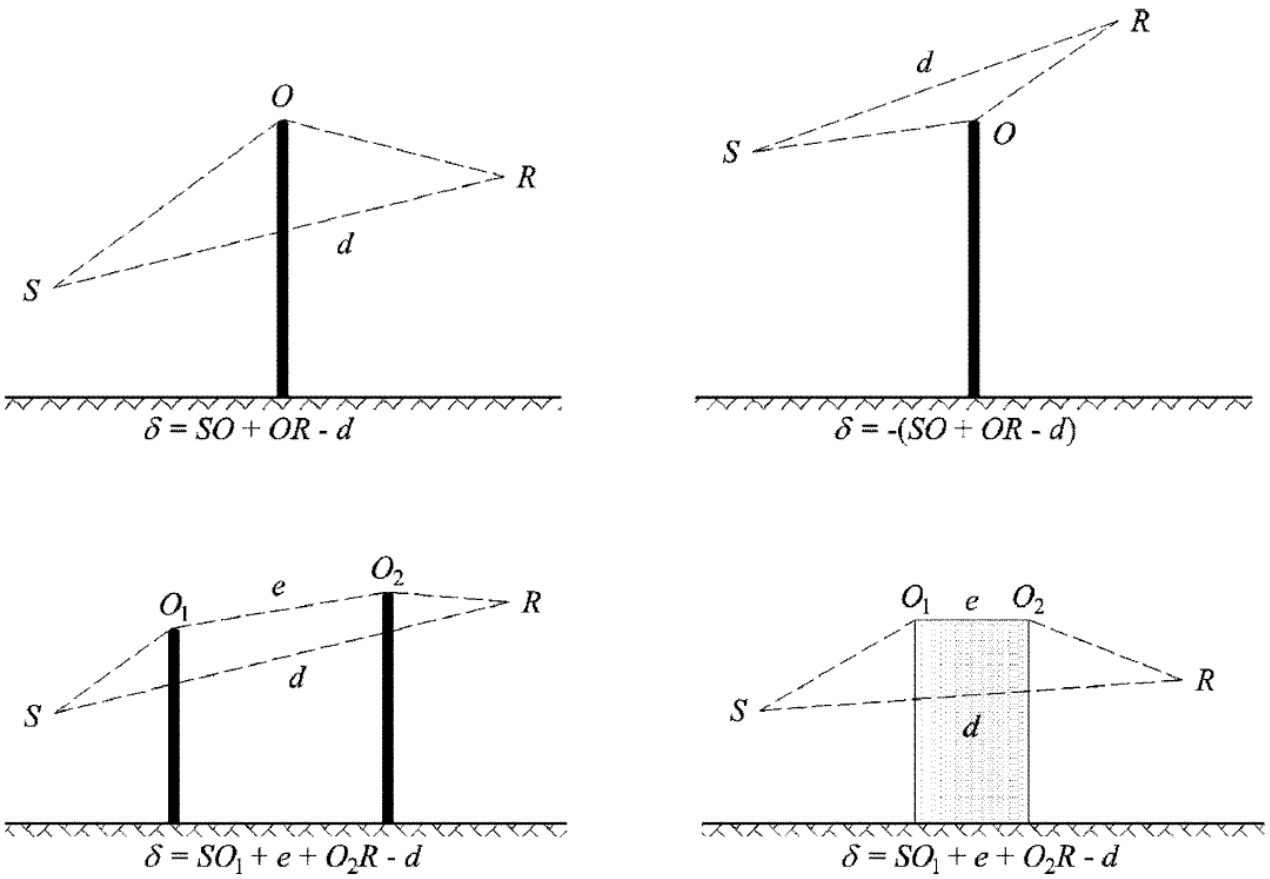

Figure 2.3. Calculation of the path difference in homogeneous conditions.

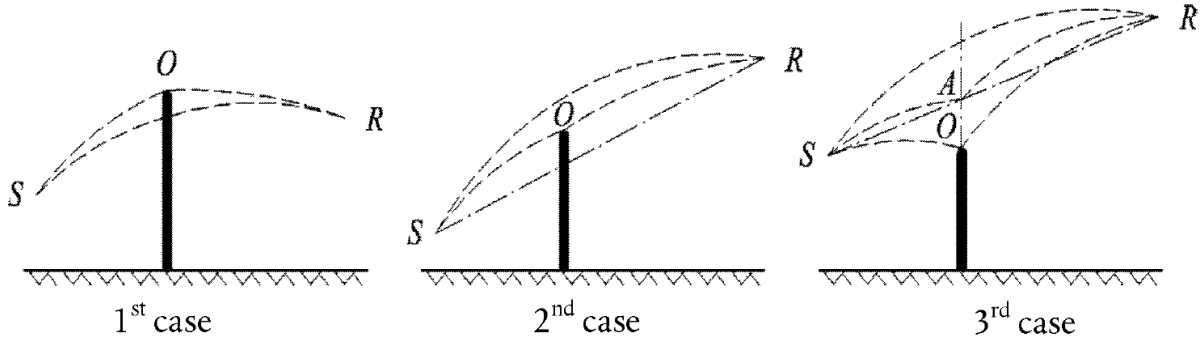

Figure 2.4. Calculation of the path difference in favourable conditions.

The last attenuation that the model takes into account does not appear in Equation (24). Instead, it is applied directly to L_{WS}, the SPL of the source. When calculating the propagation paths, if a path has reflections on vertical surfaces, the SPL of the image source, $L_{WS'}$, is obtained from:

$$L_{WS'} = L_{WS} + 10\log(1 - \alpha_r) \tag{31}$$

where $\alpha_r \in [0,1]$ is the absorptive coefficient of the surface. Equation (31) can be applied multiple times to the same source, if multiple reflections are found in the path to the receiver.

3. State of the Art

As previously stated during this work, noise simulation in urban environments is an active field of study, which means that there are still new models, methods and tools being developed currently. Nevertheless, all present works are related to one or more of the methods reviewed in the previous section.

Iu and Li [22] studied the propagation in narrow street canyons through an analytic Green's function. The Green's function is a particular formulation of the wave equations in the frequency domain that does allow wide angle scattering and even backscattering [10], unlike the typical frequency-based methods as discussed at the end of Section 2.1. The analytic function used, however, is simplified through multiple simplifications that reduce the scope of the method: the source and receiver are placed between vertical infinitely high walls, completely reflective; the ground is flat and horizontal, and is the only surface with impedance; and the street canyon is infinitely large. Results were validated through experimental results obtained inside an anechoic chamber with reflective surfaces placed inside, obtaining a good agreement between results. Still, the method is very limited to an ideal case.

The most popular option when using wave-based methods is to use FDTD, as it models all the frequency range, allowing to obtain broadband solutions with high accuracy. Still, computing large domains requires significant is costly computationally, both in terms of power and in terms of storage. As an example of order of magnitude, Parker *et al.* [14] performed a study of a fictitious city district of 750×750 m^2 containing 2–3 story buildings with a point source close to the floor. The resultant mesh had 2.736e9 nodes. This simulation was carried out in a cluster with 256 processors and took 5 h 59 min. This can appear not that high, but it has to be considered that the source simulated produces a Gaussian pulse with a 40 Hz centre, and only frequencies up to 91.6 Hz are calculated. These frequencies are extremely low; both ground vehicles and UAVs emit noise at much higher frequencies, hence the mesh should be much more refined. Because of this reason, multiple studies have focused on developing highly efficient numerical codes to reduce computation times.

Van Renterghem *et al.* [12] developed a solver to compute sound propagation between two city canyons coupling FDTD and PE. In this case, FDTD is used to calculate the field inside of the city canyons, and propagation above roofs is performed by a PE solver, which is more efficient. This solver is used to compute a 2D case, illustrated in Fig-

ure 3.1. It is possible to use a PE above the roofs because there are no reflections outside the propagation path in this case, unlike inside the canyon. The solver first calculates the FDTD region, which is surrounded by a PML in order to simulate a free propagating wave outside the canyon. Data is recorded along a line, where the PE field is started in the next step. The PE, nevertheless, is a frequency-based method, so a FFT is used to change between domains. The field is calculated only until the symmetry plane is reached. The symmetry of the geometry is exploited in the calculations: if the receiver is placed in the location mirroring that of the source, the transfer function between the source and the symmetry plane is the same as the transfer function between the symmetry plane and the receiver. Obviously, this makes this method rather limited: only a point is calculated at the receiving canyon, and it has to be placed symmetrically.

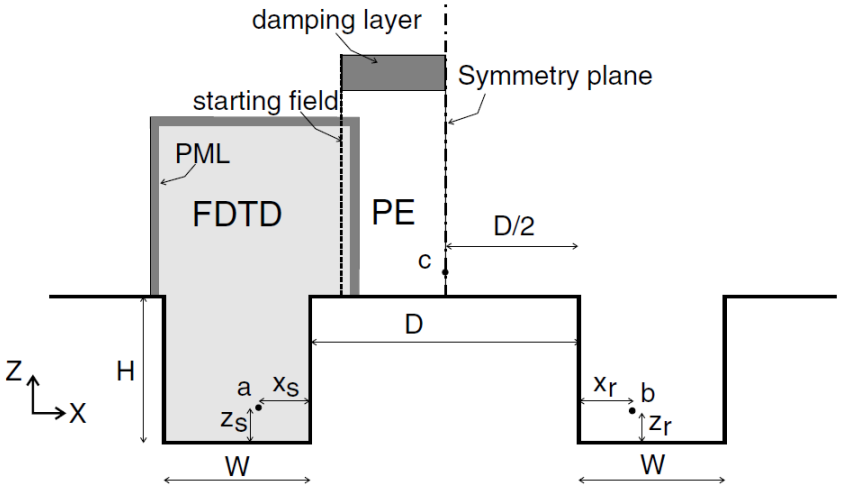

Figure 3.1. Geometry and regions of the FDTD-PE simulation [12].

Instead of coupling with other methods, Montanaro *et al.* [13] propose a parallelized scheme accelerated by GPU. In this case, the underlying equations are Equations (1) and (2), already discussed in Section 2.1. Efforts have been dedicated to optimizing the calculation process by slicing the 3D domain in 2D slices (or the 2D domain in 1D slices) with each GPU (with 24GB of memory), with overlapping layers between each 'adjacent' GPU. Indeed, one of the most limiting factors that highly increase computation times is the amount of global memory, since the entire pressure and velocity fields need to fit in memory. Slicing the domain allows the GPUs to compute and then store data mostly independently. Using this method, each slice of a 2D domain of 160×20 m^2 is computed in around 6 minutes, using a mesh that can resolve frequencies up to 2 kHz.

A completely different approach was developed by Raghuvanshi *et al.* relatively recently (2009) [11], and later expanded in [30], method coined as Adaptive Rectangular De-

composition (ARD). This method was developed with the aim of allowing to obtain data for sound rendering in different soundscapes inside of virtual environments, performing all calculations on a desktop computer, yet achieving a high accuracy. This method allows to compute the results taking an order of magnitude less memory and two orders of magnitude less computation time than a standard FDTD method, even achieving in some cases a more accurate result. This method is still based on the acoustic wave equation, but in the case with homogeneous conditions and no speed (Equation (3)), and it takes advantage of the fact that the analytical solution to the wave equation within a rectangular homogeneous domain is known, allowing good results even in coarse meshes, close to the Nyquist limit (only 2 samples per wavelength instead of 10). Furthermore, inside these rectangular domains the solution can be calculated using a Discrete Cosine Transform (DCT), which can be calculated very efficiently using a FFT. As the solution used inside the rectangular domains is analytical, no numerical dispersion is added in the propagation, only at the interfaces between rectangular regions, where an Inverse DCT and a DCT are applied. The pressure signals at the interfaces are used to compute a force that will enter the following air partition. The ARD has been validated in [31] and [32], obtaining in both cases a good agreement between simulated and experimental results. The downside of this method is that it cannot simulate inhomogeneous moving media. Still, it is still a really powerful model.

Regarding works that have focused specifically on UAVs over urban areas, Casalino *et al.* [33] carried out a simulation of a helicopter flying over an urban area. The pressure field on the rotating blades is computed using an unsteady BEM solver. The blades are then used as a source, and the sound propagation close to the helicopter and in the nodes belonging to its fuselage using the Ffowcs Williams and Hawkings (FW-H) analogy (time-domain). The results are propagated up to an interface with a different mesh. FFT is then used to convert results to the frequency-domain, and a FEM solver is used to propagate the results both inwards and outwards the interface, with a jump condition at the interface. The whole acoustic simulation using one processor of a laptop requires 3 hours for the first frequency and 2.5 hours for the subsequent ones.

A related work is [34], in which instead of FEM, a BEM solver accelerated with Adaptive black-box Fast Multipole Method is used. Similarly to [33], a free-wake vortex lattice BEM solver is used to solve the aerodynamic problem, and the FW-H analogy is used to propagate sound in the near free field, obtaining a spherical source for the BEM acoustic solver, yet again in the frequency-domain.

Yunus *et al.* [25] used a GBT in-house code named UYGUR to simulate a VTOL aircraft overflying an urban area. A sphere of noise is obtained from Blade Element Momentum Theory (BEMT). This solver also incorporates weather data from another CFD simulation done beforehand, from which wind profiles are obtained. The solver is validated with a FEM simulation, with a good agreement between results, except from points between two adjacent buildings, due to the sound waves diffracted into the building canyons not being present in the GBT simulation.

A similar study was carried out by Tan *et al.* [35]. Like in [25], a BEM method is used to obtain a spherical source from the UAV. GBT is then used at different stages of a flight path of study. Different payload and speed configurations are studied, but in this case no whether data is considered. Nevertheless, unlike [25], [33], [34], not all surfaces are completely reflecting, and the effect of vegetation covers on the weighted SPL is studied.

Both [36] and [37] compute noise maps produced by a UAV using commercial software iNoise, which uses the calculation methods described by ISO 9613. These are the same methods that CNOSSOS-EU uses. The propagation method described by ISO 9613 was selected for CNOSSOS-EU over two other methods: NMPB 2008 and HARMONOISE [38]. In [37], the UAV noise measurements were performed as explained in ISO 3744, in which methods for measuring outside an anechoic chamber are described. Furthermore, in the same study results were validated against experimental results. A good agreement between measured and calculated SPLs were achieved ($\pm$2.1 dB (A)), proving that the low computational effort methods described in CNOSSOS-EU/ISO 9613 can be used for noise mapping confidently in a large variety of circumstances.

Before proceeding with the review of the solvers available to the public and some examples of noise emission calculations, it is worth noting that most of the works reviewed considered all surfaces to be completely reflecting [11], [14], [25], [30], [31], [32], [33], [34], [36], [37]; and none of them had a moving source. Instead, for the studies regarding VTOL aircraft a flight condition was considered and a spherical or point source was computed from it [25], [33], [34], [35], [37]. Studies involving FDTD simulations were carried out in 2D domain due to time or memory limitations [12], [13] or had large clusters at their disposal [14]. Studies using FEM or BEM, also computationally costly, resorted to perform simulations in the frequency-domain, calculating then only tonal noise from the rotorcraft [33], [34] (Blade Passing Frequency – BPF – and its harmonics).

There is a clear limitation in the wave-based methods, specially in time-domain that make then unviable for a lot of researchers. Adaptive Rectangular Decomposition, being

relatively new when compared to the other methods (all other methods were described in the twentieth century, while first article formulating ARD is from 2009), has still little background, and is currently limited to non-moving homogeneous media. This leaves as prime candidates GBT and ISO 9613/CNOSSOS-EU, for research focused simulations and practical uses practical applications respectively. In any case, computational power has vastly increased in the later year and GPU-based numerical methods are becoming more and more efficient, so it is possible that FDTD, or time-domain FEM and BEM, become viable options in the near future.

4. Methodology

In Section 3 of this thesis, a description of current work and developments in the field of sound propagation in urban areas has been provided. The main goal of this work, nevertheless, is not only to be comprehensive introduction to this field of study to those who do not know it, but also to assess the tools that are available to researchers currently to perform this kind of simulations. From the software that are reviewed below, two options were selected to carry out simple simulations that prove the strengths and weaknesses of the methods used by them: openCFS [39] and NoiseModelling [40].

On the other hand, for the simulations that have been carried out, data of the noise directivity of a XOAR PJN 9X7" has been used. This data is the result of transient and compressible CFD simulations coupled with the FW-H analogy [41]. Data were also validated in an anechoic chamber with a wooden propeller.

4.1. Available software

Most of the studies reviewed during Section 3 use numerical codes that have been developed explicitly for the studies described or use in-house solvers, the exception being those that used the commercial software iNoise [36], [37], which offers a free license that allows to perform calculations of small models in 2 cores with the ISO 9613 methods. Premium licenses of the software also include model HARMONOISE, which is arguably more precise, as it allows to model specific meteorological conditions and takes into account discontinuities in the ground impedances, instead of averaging them, though it is also more computationally demanding [38]. Nevertheless, only capabilities included in the free license have been taken into account, as the focus of this work is on open-source software.

Regarding wave-based methods, there are multiple options available. Software PFFTD, developed by Brian Hamilton [42], is an implementation of FDTD for 3D simulations, designed to run on a Linux system. This software is design to run on Nvidia GPUs using CUDA for efficient parallelization to perform high precision simulations in broad spectrum of frequencies (16 Hz to 16 kHz). The scripts of this program, however, are design for room acoustics, and although equations are the same, meshing process is carried out by the Python scripts included in the program, which has not been designed for this purpose. More importantly, no implementation of PML is found in the software, as it is usually not required in room acoustics.

Another similar option, but focused on open domain problems, is openPSTD [43], [44], an implementation of the Fourier Pseudospectral Time-Domain (PSTD) method. PSTD has the advantage of allowing to use coarse meshes close to the Nyquist limit without adding much numerical errors (note that coarser meshes also allow to increase the timestep of simulations). The software is built using Blender, Numpy and Python, and allows the possibility of accelerating calculations by partial implementation of the code on the GPU. The biggest downside of this software is that, as of the date this work is being written, documentation is no longer available.

The last option implementing wave-based methods considered has been openCFS [39], an open-source software for couple field simulations (hence the name) using FEM implementations of the different PDEs. Among the different models, openCFS includes an acoustical model [45], though it only considers homogeneous media and does not allow to implement whether conditions (the PDE included is Equation (3)). However, it has the possibility of coupling the acoustic simulations with CFD to produce accurate sound sources. It also can perform mechanic-acoustic coupled simulations using no external programs. Most importantly, openCFS is currently an active project, with plenty documentation, and one can expect new features to be added progressively.

Concerning software that uses GA, i-Simpa [46] was developed as a Graphical User Interface (GUI) to host different numerical codes for sound propagation in complex environments. It also includes two solvers: TCR, based on the classical theory of reverberation, and SPPS [47], a sound particle tracing method. The latter code is the most suitable of the two for open domain simulations, and SPPS allows to apply absorption coefficients for different frequency bands to different surfaces, and also scattering indexes. The scattering indexes are used to choose statistically if a reflection of a particle should be specular (angle of reflected ray is the same as the that of the incident one) or diffusive (in a 'random' direction). Diffraction, sadly, is not modelled in the code. However, it does have extensive documentation, though all tutorials are applied to cases of room acoustics.

Code_TYMPAN [48] is a software developed to simulate noise in industrial sites through raytracing (not GBT). The numerical code also accounts for diffraction, creating new rays when a ray passes close to an edge. The program comes with a GUI and docu-

mentation can be found, although, to the best of the author knowledge, only in French[1]. The project is still being updated currently, so improvements are to be expected.

The last of the software that were considered is NoiseModelling [40], a tool designed to produce environmental noise maps on very large areas using the methods of CNOSSOS-EU. NoiseModelling can be used as a Java library or controlled through a web interface from which nodes with parameters are defined and processes then launch. Plenty documentation and tutorials are available, and the software is compatible with all relevant file types used in cartographic fields (shapefile, GeoJSON, CSV…), which makes it compatible with any GIS software.

Table 4.1 and Table 4.2. contain a summary of the features reviewed above:

Software	Wave-based/GA	Model	Phenomena
PFFTD	Wave-based	FDTD	Reflections and diffractions. No PML.
openPSTD	Wave-based	PSTD	Reflections and diffractions. Atmospheric absorption. Can model the effect of wind.
openCFS	Wave-based	FEM	Reflections and diffractions. Atmospheric absorption.
i-Simpa	GA	SPPS	Specular and diffusive reflections. Sound transmission through walls. Atmospheric absorption. No diffraction.
Code_TYMPAN	GA	Raytracing	Reflections and diffraction.
iNoise	GA	ISO 9613	Reflections and diffractions. Atmospheric absorption. Estimation of whether effects.
NoiseModelling	GA	CNOSSOS-EU	Reflections and diffractions. Atmospheric absorption. Estimation of whether effects.

Table 4.1. Summary of sound propagation methods used by software and the phenomena they can simulate.

[1] As it has proved somewhat difficult to find, the following URL is provided: https://github.com/FDiot/code_tympan/blob/master/doc/_static/documents/User_Manual-fr.pdf

Software	Documentation	GUI (Y/N)	State
PFFTD	Outline explanation by the developer on GitHub.	N	Last update 3 years ago.
openPSTD	No longer accessible.	Y	Last update 8 years ago.
openCFS	Accessible. Tutorials and different applications. A testsuite can be also found online.	N	Project currently active and receiving updates.
i-Simpa	Accessible. Tutorials available.	Y	Project currently active and receiving updates.
Code_TYMPAN	Only in French.	Y	Project currently active and receiving updates.
iNoise	Accessible. Tutorials available in video format.	Y	Commercial software.
NoiseModelling	Accessible. Tutorials available.	Y	Project currently active and receiving updates.

Table 4.2. Summary of user-friendliness features of reviewed solvers.

For this work, it has been deemed suitable to perform both simulations with wave-based methods and with GA methods. From the software listed in both Table 4.1 and Table 4.2., openCFS and NoiseModelling were selected. This is due to both of them having good capabilities when modelling the different phenomena, but also due to their accessibility to new users: NoiseModelling has GUI and even if openCFS does not, the available documentation makes it easy to understand the architecture of simulations.

4.2. Set up of the openCFS simulations

For the openCFS simulation, due to memory and computation limitations, the simulations have been performed in 2D domains. Still, the configuration of 3D simulations is exactly the same, so these serve as an example of how the software is used. Besides, 2D simulations can still be used to study the effects of reflections and refractions on the perceived SPL.

The simulation file of openCFS is an XML based input format, in which the geometry, the properties of the medium of propagation, the analysis type and the PDEs to use

have to be stated. Most cases' set ups will require at least 3 files: the mesh file, the material file and the simulation file itself.

Starting for the mesh file, openCFS is compatible with Ansys CDB (used by the ANSYS APDL, but also by cubit and trelis), and Gmsh. Only the latter comes from an open-source software, so it has been the choice for this project. Gmsh [49] is an open-source 3D finite element mesh generator that supports CAD formats and also has its own in-built CAD engine. The program has a GUI to write files in its own scripting language, which can be also accessed and edited with any text editor. The case that has been studied is a UAV (modelled simply with the XOAR PJN 9X7" so that the sound source is axisymmetric) hovering over a street canyon, next to another street canyon, as seen in Figure 4.1. The specifications of the geometry are displayed in Table 4.3. The goal is to study the difference between the SPL perceived at each canyon, which is not a trivial question due to the directivity of the tonal noise.

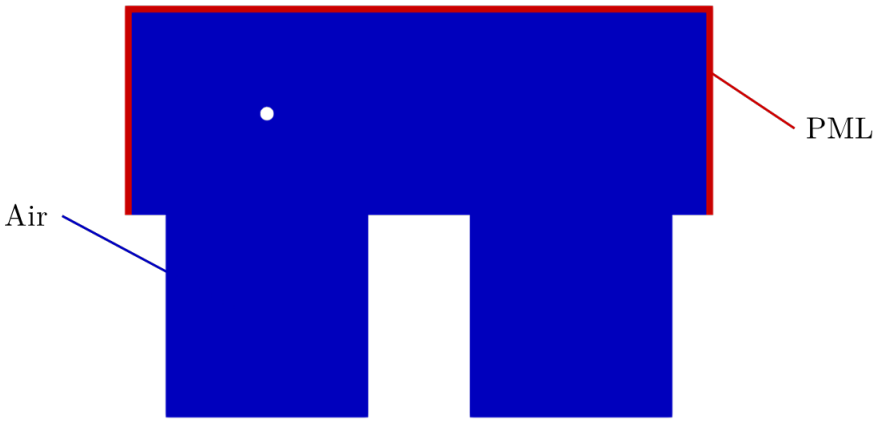

Figure 4.1. Geometry for the openCFS simulation.

Streets width [m]	30
Buildings height [m]	30
UAV height [m]	45
Middle building width [m]	15
Left and right buildings width [m]	5
Domain height (no PML) [m]	60
PML thickness[m]	**1**

Table 4.3. Geometry of the openCFS simulations.

The mesh will be used in a case with pure tonal noise, so that it can be solved in the frequency-domain, though time-domain simulations will also be performed. The discretization of the mesh has to ensure that there are at least 10 elements per wavelength. Frequencies of interest are the Blade Passing Frequency (BPF) and its first harmonic, for frequency-domain simulations, and only the BPF for time-domain methods. The decision to only simulate the BPF in time-domain has been done to allow the use of a coarser mesh, since coarser meshes also allow to increase the timestep. For a rotational speed of 7375 rpm, the frequencies are respectively 245 Hz and 490 Hz, hence, if the speed of sound at 20 °C is 343.25 m/s, the spatial discretization cannot be larger than 0.07 m. To facilitate the realisation of a structured mesh, 0.05 m was chosen instead for the frequency-domain simulations. The mesh used for time-domain simulations uses a spatial discretization of 0.1 m instead. The PML thickness has been selected taking into account that, according to the documentation, the PML elements should be of the same size that those of the propagation region, and there should be at least 4 first order elements. The meshes produced had 20 and 10 (for the frequency and time-domain simulations respectively) instead, to ensure that even at the points of the domain where the impinging wave is almost parallel to the domain (the PML is most effective when the impinging wave is normal to the boundary), the PML avoids reflections.

Gmsh allows to create structured quad meshes using transfinite curves and surfaces. This process requires compartmenting the domain in surfaces with exactly 4 boundaries, as shown in Figure 4.2. The number of elements across each edge is specified and then the mesh is produced (see Figure 4.3.). Using 0.05 m of spatial discretization, a mesh with 3.8364e+06 elements has been obtained, whereas when using 0.1 m it resulted in only 898500 quadrangles. Note that, in order to maintain an aspect ratio close to 1, elements close to the UAV are much smaller (≈ 0.00235 m and ≈ 0.00470 m).

Before exporting the meshes, the different regions that will be present in the simulation have to be defined. In order to do so, al surfaces that correspond to 'Air' in Figure 4.1. must be group in a physical group. Same for the PML. It is also necessary to include the curves of the circumference that corresponds to the UAV, as a boundary condition has to be defined at it.

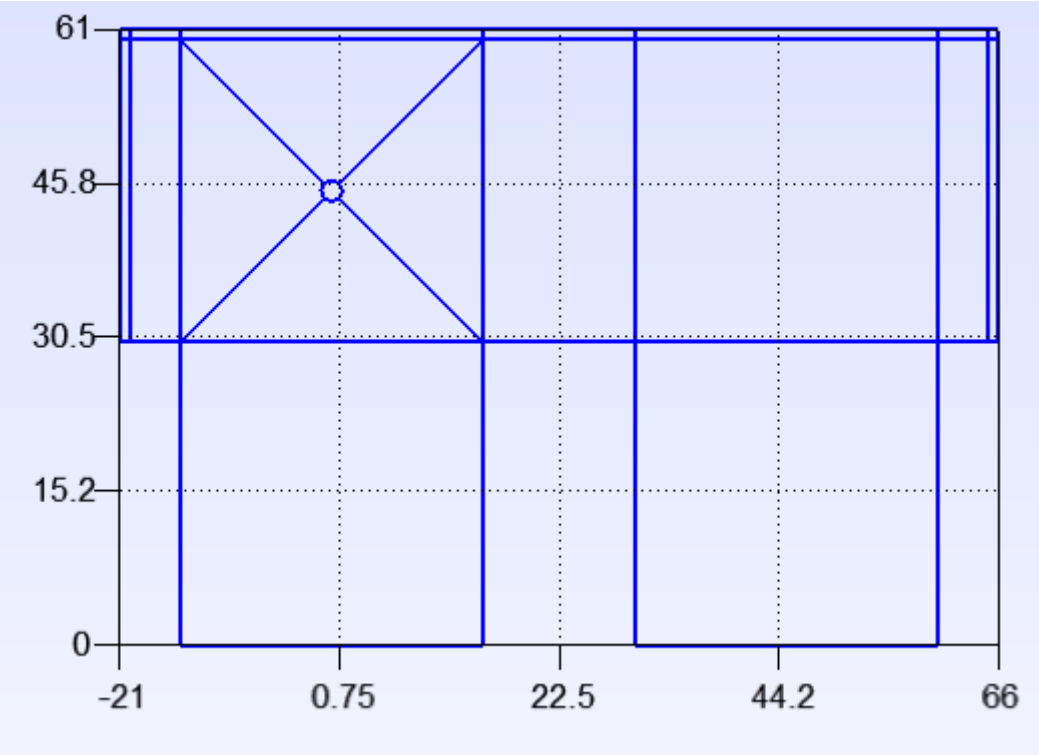

Figure 4.2. Geometry defined in Gmsh. Surfaces must have 4 boundaries to produce a transfinite structured mesh.

Once all regions and boundaries have been labelled, the meshes can be exported. OpenCFS is compatible specifically with the default Version 2 ASCII (if 'Save all elements' or 'Save parametric coordinates' are checked, the software will not recognize the structure of the file).

Regarding the material file, it only needs two values. The density ρ and the compression modulus K, which are used to compute the speed of sound c_0:

$$c_0 = \sqrt{\frac{K}{\rho}} \tag{32}$$

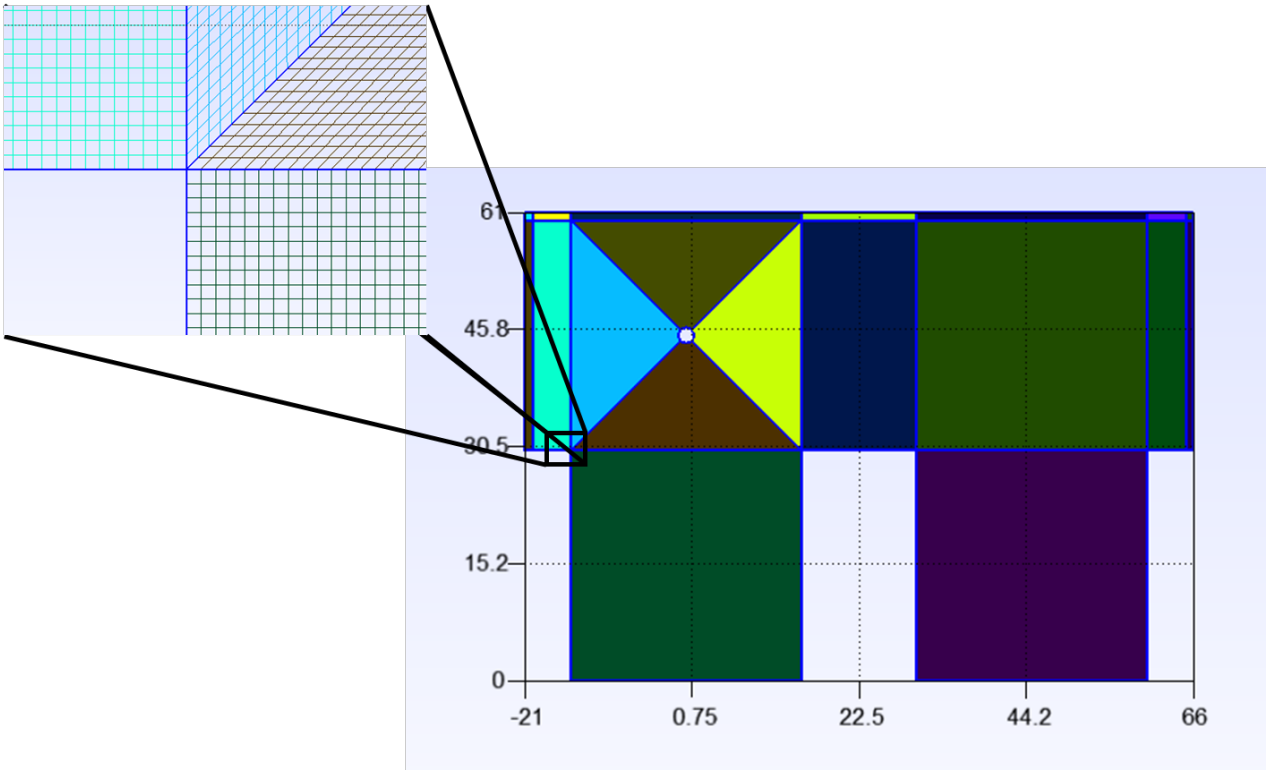

Figure 4.3. Mesh for frequency-domain simulations produced by Gmsh.

Values of the three variables at sea level and 20 °C are provided in Table 4.4. Only the first two have to be included in the acoustic material file.

ρ [kg/m^3]	K [MPa]	c_0 [m/s]
1.204	0.141855	343.25

Table 4.4. Air properties at sea level and 20 °C.

Before describing the simulation file, the obtention of the directional source will be discussed briefly. Data used for this purpose comes from [41]. From the data that was available, the results of the URANS simulation were used, which do not model correctly the broadband noise, but they do provide accurate results for the tonal noise, at least the first harmonics. The results were propagated to a 2 m radius sphere with the FW-H analogy. The SPL at the frequencies of interest was extracted, and the acoustic pressure for the simulation obtained from them. In order to introduce acoustic pressures in the simulation, polynomials have been fitted. The resulting functions have been introduced in the definition of the boundary condition. This is possible because from the simulation file it is possible to access the variables of the simulation (in this case, the coordinates and the frequency) and use them to define functions. Figure 4.4. shows the acoustic pressures obtained with the simulations together with the fitted polynomials that were used in the simulation

files. On a side note, it can be seen that the tonal noise is much lower above and below the propeller.

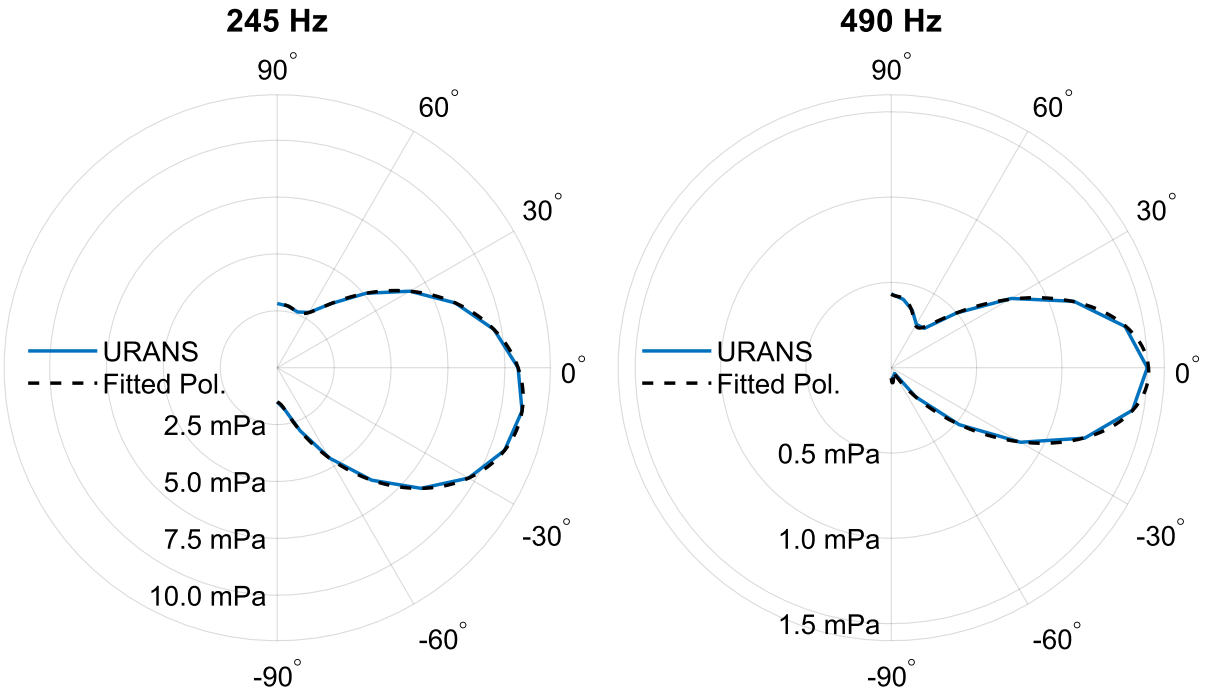

Figure 4.4. Simulated and fitted directivities of the acoustic pressure of a XOAR PJN 9X7" propeller at the BPF and first harmonic when rotating with angular frequency of 7375 rpm.

Finally, regarding the simulation file, first, the input and output files are specified. The input files in this case are the mesh and the acoustic material file. The output is a hdf5 file that can be accessed after the simulation is completed with ParaView to post-process the results. Next, the domain is specified with a list of the regions that will be used, and which material properties they have (all have been set to 'air', as this is the only propagation medium considered). A list of variables that will be used in the file other than the ones that the program already keeps track of can be included in. For example, in this simulation, the coordinates of the UAV have been listed because they are needed to define the acoustic pressure directivity at the source boundary.

Afterwards, the analysis type is specified. Both transient and harmonic analysis have been performed. Transient simulations were performed with a timestep $\Delta t = 10^{-4}$ s. In the propagation region, the Courant-Friedrichs-Levy number is 0.34:

$$CFL = \frac{c_0 \Delta t}{\Delta x} = \frac{343.25 * 10^{-4}}{0.1} = 0.3432$$

Lastly, the PDEs and boundary conditions are established. The simulations performed use the PDE referred internally as 'acouPressure', that has to be applied to regions 'AIR' and 'PML'. For the region 'PML', a damping ID is used. This ID assigns to the region the properties defined in the 'dampingList', in which the PML method is defined (inverse distance with damping factor of 1). The boundary conditions are next, and only the UAV emission has to be defined, as due to the FEM formulation of the PDE, all boundaries with no conditions are equivalent to perfectly reflecting surfaces. Like in multiple of the works reviewed in Section 3 [25], [33], [34], the boundaries are not assigned an impedance because brick, concrete, asphalt, and most building materials have really high impedances, that when taken into account, affect slightly the results. Still, defining an impedance value can be done simply by using the impedance boundary condition and setting a value for the real and imaginary components, but modelling the complex impedance is not a simple task. To store results, at the end of the solver definition it is specified the variables that want to be store and at which points. The acoustic pressure has been stored in all nodes from all regions.

4.3. Set up of the NoiseModelling simulations

For the NoiseModelling simulations, a case of a point source (the UAV) with directivity in a large urban area will be considered, as CNSOSSOS-EU methods allow to compute large areas in short timeframes.

Similar to the openCFS simulation, the geometry definition is the first step. The city of Benidorm has been selected as the domain, as in the near future experimental data will be recorded as part of national project MODERA, allowing to validate simulation results.

NoiseModelling structures all data in tables that can be imported from, and exported to, a broad selection of formats. For a simulation of a point source with directivity, four tables are required: 'buildings', 'ground', 'directivity' and 'source'. The first table contains the coordinates of the polygons' vertices that represent the buildings as seen in top view. It also contains their height. The table 'ground' contains the coordinates of the polygons that form the absorptive ground patches and the respective values of the absorptive G coefficients (see Section 2.3.). Table 'directivity' stores values of attenuation in dB for the point source at different latitude and longitude positions (angles 'Theta' and 'Phi' respectively). Attenuation values have to be provided at 5° intervals. Lastly, the table 'source' contains the coordinates of the point and the SPL at different frequency bands (LW63, LW125, LW250, LW500…). Besides the data described, all tables have a PK or primary key field, which is used as an ID for the different elements of the table.

Defining all these data from scratch would not only be incredibly time consuming, but also hard to do, as the height of all buildings in the domain of calculations needs to be specified without the possibility of taking measurements by oneself. Luckily, NoiseModelling is compatible with OpenStreetMap (OSM) [50], an open database licensed under the Open Data Commons Open Database License. Data from the database can be easily extracted using BBBike.org [51]. The area of interest can be chosen at this web page, and a file is then sent to the provided email address. This file contains all data necessary regarding buildings, ground and roads (in case it is desired to simulate the noise produced by traffic using the CNOSSOS-EU methods). Once data has been imported to NoiseModelling, it can be exported as a GeoJSON file to open it in a GIS software, where post-processing and closer examination can be made. For this work, open-source program QGIS [52] has been used. As shown in Figure 4.5., the vectorial layers match the satellite view of Benidorm, validating the imported geometry.

Figure 4.5. Comparison between satellite image and the OpenStreetMap database geometry (Benidorm).

QGIS is not only used for post-processing; layers can be created and then exported. A table of attributes can also be defined for these layers. A new layer formed by a single point was created in QGIS. Its attributes are shown in Table 4.5. Note that the fields 'YAW', 'PITCH', 'ROLL' and 'DIR_ID' are only necessary to compute define the di-

rectivity of the sound source. The former 3 describe the orientation of the sound source, and the latter is an identifier of the directivity sphere. The UAV is considered again to be hovering, hence the null values of the Euler angles. Note that the source is axisymmetric (only a propeller is being considered), hence the yaw angle does not affect results.

PK	LWD250	LWD500	YAW	PITCH	ROLL	DIR_ID
1	71.8 dB	54.5 dB	0	0	0	1

Table 4.5. Attributes of the UAV point source.

Like in openCFS simulations, the source has been modelled through the SPL results obtained from URANS simulations for the BPF and its first harmonic (245 Hz and 490 Hz) [41]. Due to SPL data only being able to be input for specific values (the centre of the frequency bands used by the software), as these frequency values are close to those of the BPF and its harmonic, they have been input directly into the closest matching frequencies: 250 Hz and 500 Hz (fields LWD250 and LWD500 respectively of Table 4.5.). LWD250 and LWD500 values of Table 4.5. are the highest SPLs obtained at the BPF and first harmonic frequencies respectively. Note that the values are higher than in the openCFS simulation, as CNOSSOS_EU works with point sources. The SPL has been corrected accounting for attenuation caused by divergence (Equation (25)). Noise directivity is then computed with the aid of a CSV file where attenuation values in dB are specified at each 'Theta-Phi' pair (thus the use of the maximum SPL in the source file). The CSV file used for directivity has been built with MATLAB using results from [41].

The point source has been placed in the part of the city where flight tests will be conducted as part of the MODERA project. Figure 4.6. shows exactly the position of the point source inside the city. Once the fields of Table 4.5. have been filled, the point source can be exported as a GeoJSON file, which can then be imported into NoiseModelling to perform simulations. UAV is expected to fly at 20 m height, so the GeoJSON was opened with a text editor to modify the Z coordinate. Alternatively, one can change the height of a source with process Set_Height inside of NoiseModelling.

Figure 4.6. Position of the UAV point source in the NoiseModelling simulation domain.

Once NoiseModelling is launched, the web GUI is automatically opened (see Figure 4.7.). From there, commands can be easily searched for and run. To perform a point source simulation, first all files have to be imported. Then, a grid of receivers is generated. NoiseModelling offers different options to generate grids. In the simulations performed for this project, a Delaunay grid 1.6 m above ground was used. Once table 'receivers' is generated, process Noise_level_from_source can be used. Note that LWD* refers to SPL during day, and no data for night or evening SPL were provided for the source, hence all three '*Do not compute LDEN_GEOM/LEVENING_GEOM/LNIGHT_GEOM table'* have to be checked. Also, to include source directivity the name of the table containing attenuation data has to be specified. Same thing happens with ground absorption effects. Other parameters that can be modified are order of reflexions, air temperature, air humidity, diffraction on horizontal and vertical edges…

Once the resultant table 'LDAY_GEOM' has been computed, isosurfaces can be calculated and exported to QGIS.

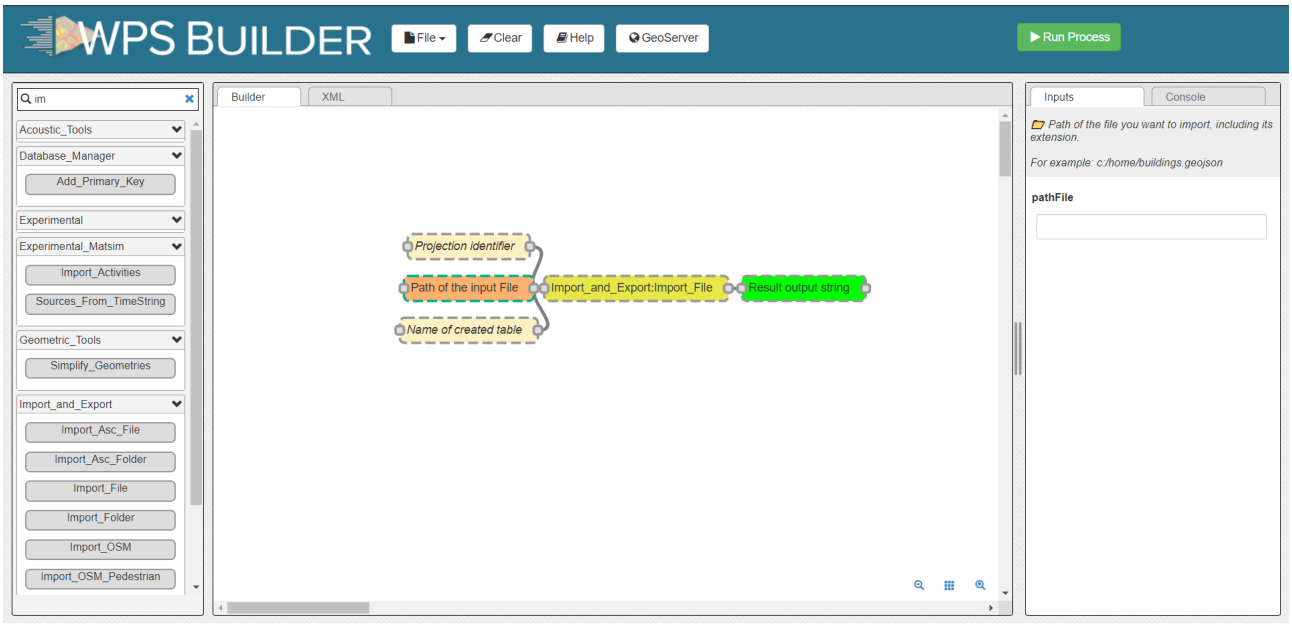

Figure 4.7. NoiseModelling's Web Page Services Graphic User Interface.

5. Results

In this section, the results of the simulations are discussed in detail. From them, conclusions about the importance of the phenomena that govern sound propagation problems will be drawn. The computational costs will also be examined briefly.

5.1. openCFS

With openCFS the goal has been to solve a problem in which the most relevant phenomena of sound propagation can be examined independently. On the one hand, the UAV hovers over a canyon emitting sound directly, but also reverberating on the walls. On the other hand, an important region of the other street canyon is masked by a building, so only the pressure coming from reflections and diffractions can get there. Furthermore, when simulating the problem in the time-domain, a diffraction wavefront is clearly formed at the upper right corner of the central building, which propagates through all the canyon before reflections from the right wall are produced.

5.1.1. Frequency-domain simulations

Frequency-domain simulations are a very efficient way of solving steady problems. Simulation time of this problem is only 3.5 minutes when launched on the 6 cores of the author's personal laptop.

Figure 5.1. shows the results of the harmonic simulation. As it can be noted, the SPL is not a uniform field that starts with high energy at the UAV and simply decays as the wave propagates away from the source. Instead, the problem is highly conditioned by the reflections, which produce patterns of constructive and destructive interference. The directivity of the UAV, which emits less tonal noise close to its symmetry axis, is also a key factor. Its effect is appreciated specially in the 490 Hz case, in which there is significantly more noise at the right canyon, even in the region directly behind the building that masks most of it.

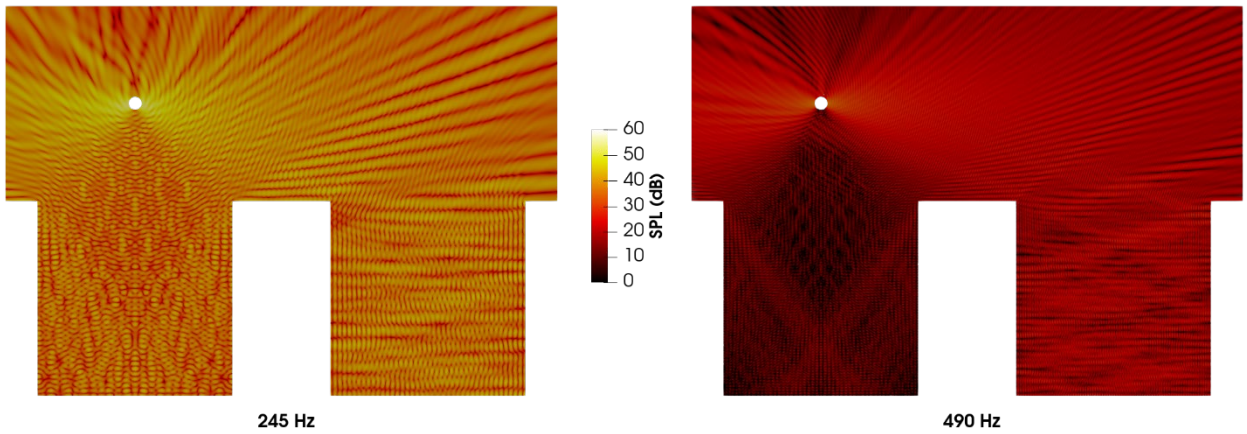

Figure 5.1. SPL field produced by the BPF and its first harmonic.

In order to make a quantitative assessment of the noise differences between street canyons, the amplitude of the acoustic pressure at both sides of the centre building have been used. Figure 5.2. shows that, whereas in the case of 245 Hz pressures are more or less equal (mean values of pressure along the façade are 2.20 mPa and 2.48 mPa for the left and right façades respectively), the mean value of pressure along the right façade in the 490 Hz case is 2.58 times that of the left one (0.28 mPa and 0.11 mPa).

Another interesting pattern is that in the left façade pressure is highest close to the top, as it is closer to the source; but in the right façade, the opposite is the case, as only diffracted waves reach that region.

On another note, the constructive and destructive interferences are closer to each other in the left façade than in the right façade (seen in Figure 5.2. as a 'higher frequency'). This is due to impinging waves impacting the surface with lower incidence at the left canyon.

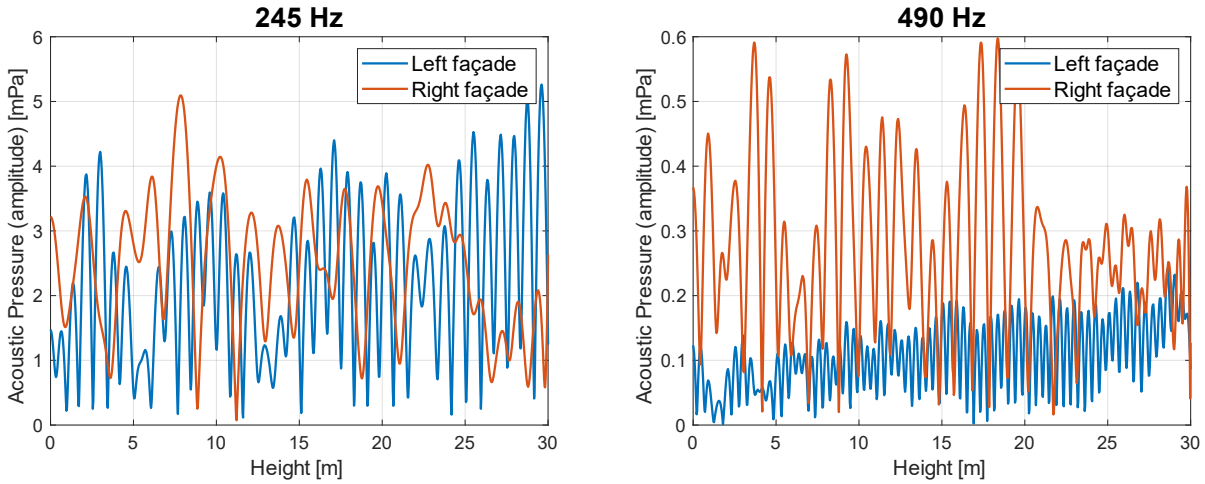

Figure 5.2. Amplitude of the acoustic pressure along the façades of the centre building

5.1.2. Time-domain simulations

Time-domain simulations are very useful to study transient problems but have incredibly high computational costs compared to frequency simulations. Not only do they require much more computation time, but also really large amounts of data are produced. Simulations performed for this section took around 3 hours and 45 minutes each to run 1 s of simulated time while running on a node of 48 cores.

Figure 5.3. shows some snapshots of the time-domain simulation of the same problem that was solved in the frequency-domain, but only using the BPF to reduce mesh elements and increase the timestep. In chronological order, one can see:

1. The wave propagates uniformly from its source.
2. Reflections take place at the walls and roofs of the left and centre buildings, creating interference patterns that start to propagate. A diffraction wavefront is started at the top right corner of the centre building.
3. The wavefront reaches the ground and start to propagate towards the source. The diffraction wavefront propagates along the right canyon. Note that the pressure of the diffracted wave is much lower than that of the original wavefront.
4. The wave reaches the right building, creating interference patterns in the right canyon.

As it can be seen, Figure 5.3. allows to visualize concepts that have been repeated throughout all this work easily. Frequency-domain simulations only show the final result, so it is harder to see how the interference patterns are exactly created. In contrast, this simulations allows to see step by step the creation of the final pattern.

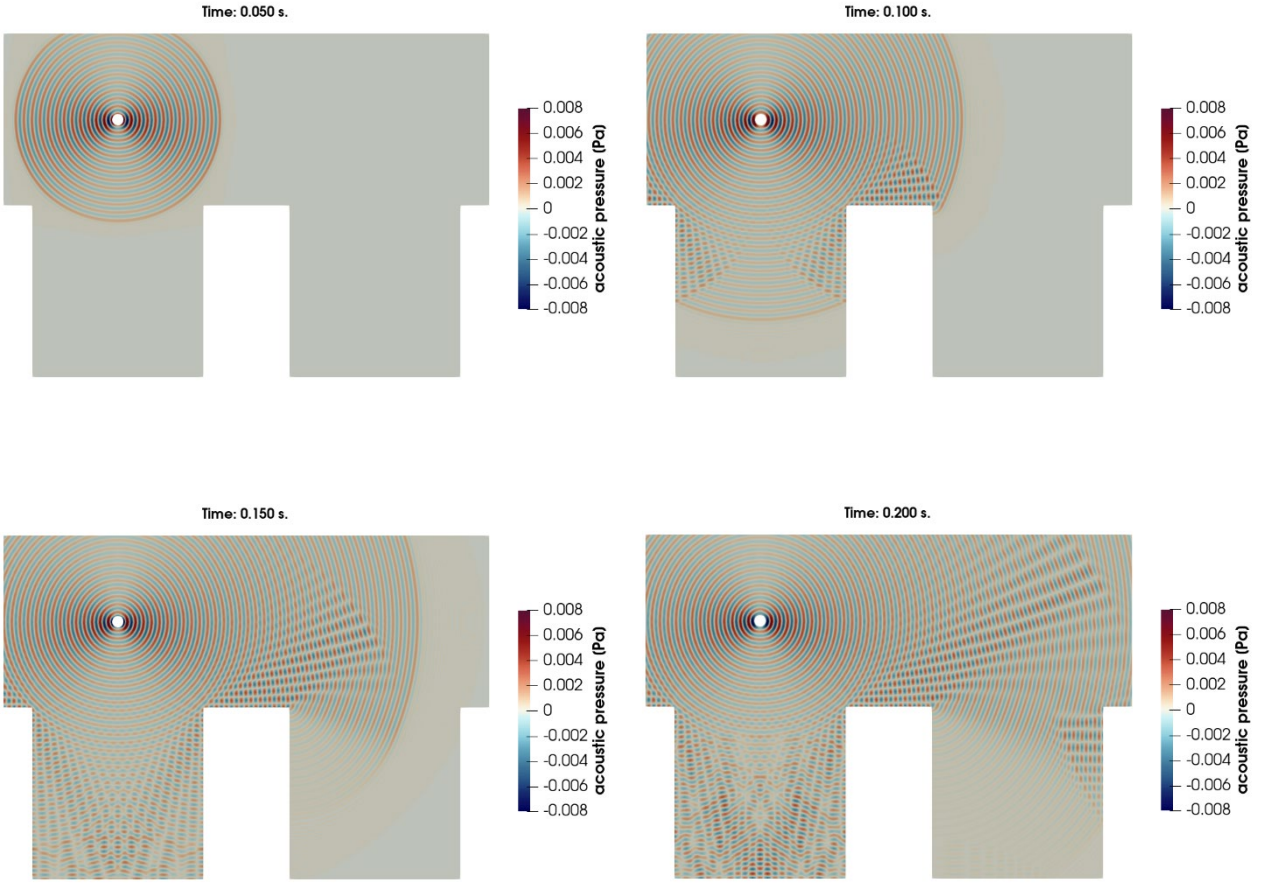

Figure 5.3. Snapshots of the time-domain simulation of the base case.

It is interesting to check that after 1 second of simulated time, the solution is almost identical to the solution obtained through the frequency-domain simulation, as highlighted by Figure 5.4. It is remembered that to achieved the left image 3 hours and 45 minutes in a 48 core processor were needed, whereas the right image was obtained in just 3.5 minutes in a 6 core processor laptop.

As reflections and diffractions are a key feature of this problem, it has been studied up to which point the results are different if no reflections are present. To do this, PMLs were added to all remaining boundaries[2]. A case in which only the ground is reflective has also been used.

[2] Regarding the implementation of the PMLs, openCFS requires that PMLs are applied to box-like domains to properly obtain the damping coefficients. To make these simulations work, multiple PML regions (three) have to be defined, so that the domain is split in bounding boxes.

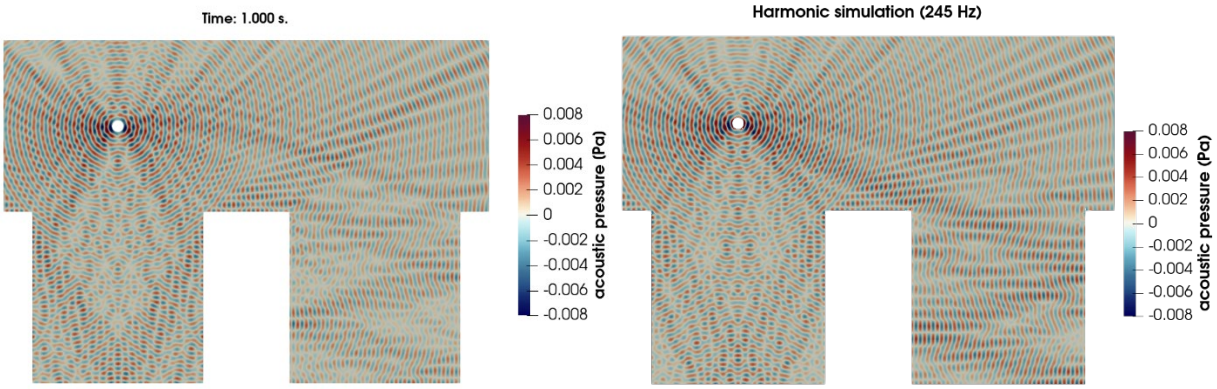

Figure 5.4. Comparison of acoustic pressure field between time-domain and frequency-domain simulations.

Figure 5.5. and Figure 5.6. show the cases with reflecting ground and with no reflections respectively. It stands out that in the places were wavefronts travel almost parallel to surfaces, the PML does not perfectly damp the wave, causing some slight interference patterns, specifically at the left canyon. Slight spurious results are to be expected.

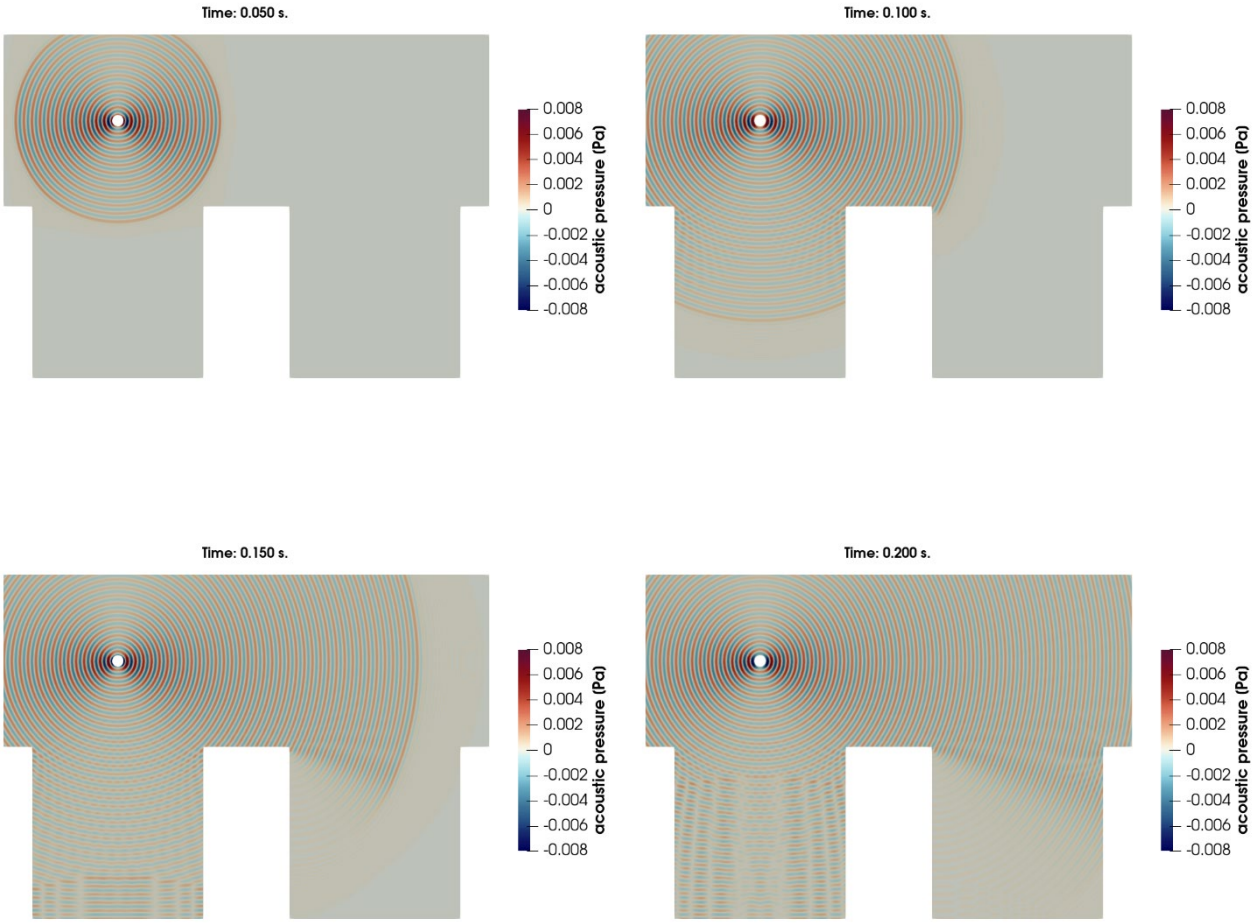

Figure 5.5. Time-domain simulation with only reflecting ground.

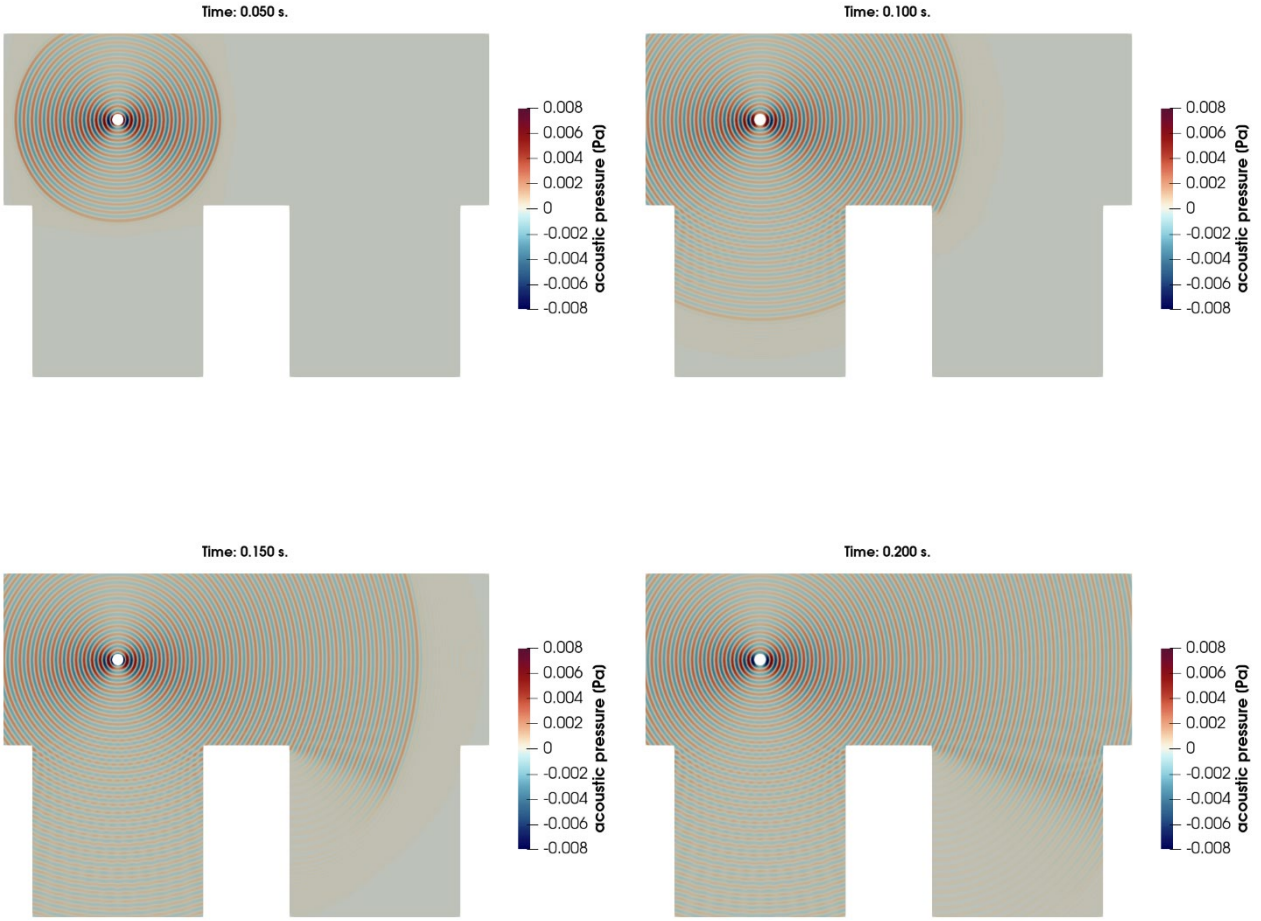

Figure 5.6. Time-domain simulation with no reflecting boundaries.

The elimination of reflecting boundaries has been done to study how big of a role they play in the resultant SPLs. Figure 5.7. shows the values of acoustic pressure measured at the bottom-centre (2.3 m above ground) of the street canyons for all three simulations. It can already be seen that the base case (with all reflecting surfaces) has the highest amplitudes, reaching 2 mPa and 1 mPa at the left and right canyon respectively. At the lest canyon, removing the reflections of the walls reduces the reverberation, halving the amplitude of oscillations, and removing also the ground halves again the amplitude. Note that no interference pattern should appear at the simulation without reflection, indicating that as it was foreseen, results have been altered by spurious effects. The relevance of reflections is even more pronounced in the right canyon, as only diffracted and reflected waves reach the bottom-centre of the canyon. Diffraction still takes place, though as reflected on the results, it produces much weaker wavefronts: results are one order of magnitude lower than in the base simulation.

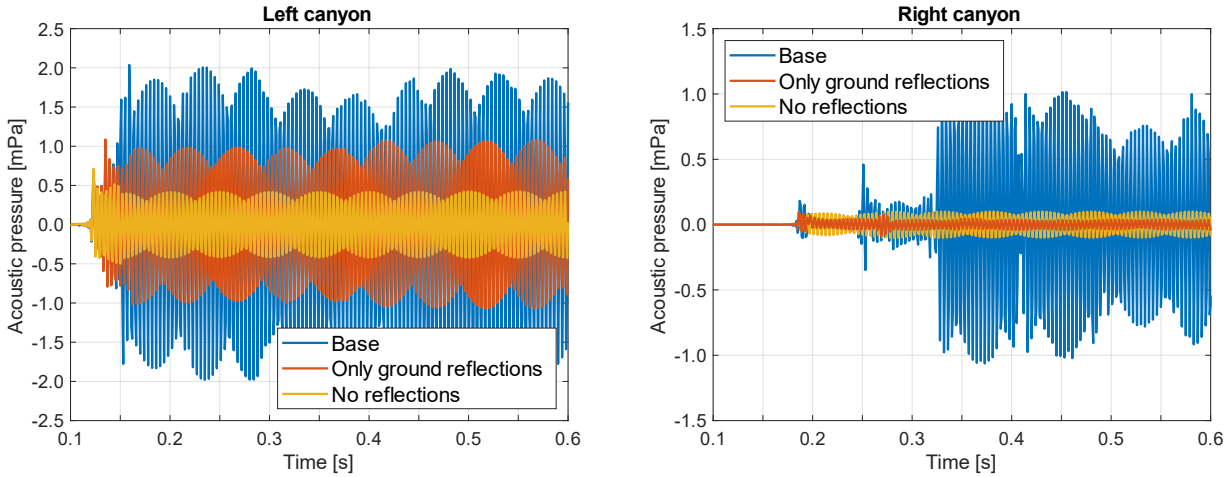

Figure 5.7. Comparison of acoustic pressure at the bottom-centre of the street canyons.

Though differences in the acoustic pressure are very pronounced, it is important to remember that human hearing works on a logarithmic scale. The transient SPL has been obtained through the time-weighted acoustic pressure, calculated with a convolution. The results are shown in Figure 5.8. In the left canyon, SPL increases monotonously until reaching the steady state value. The base case reaches in 35.5 dB, whereas the case with no reflection on walls reaches 31.6 dB, an almost 5 dB difference. In the case with no reflections the SPL drops to only 23.5, a 10 dB difference with respect to the original set up. In the right canyon something interesting happens, the SPL increases in steps. In the original simulation the wave first reaches the receiver due to diffraction, afterwards the reflected wave coming from the right wall reaches the point and lastly the wave reflected by the left wall. All three components produce a final SPL of 30.1 dB. The case with only reflections has a little bump after the wave reflected on the ground reaches the receiver, whereas the case with no reflections increases monotonously. There is a difference of almost 20 dB between the base case and the one with no reflections, and almost 28 dB with the case with reflecting ground. As for the answer to why at the right canyon the case with no reflections has a higher SPL than the one with reflecting ground, it could be that the interference pattern creates a point with low noise precisely at the receiver, or maybe it is due to spurious effects introduced by the extra PMLs.

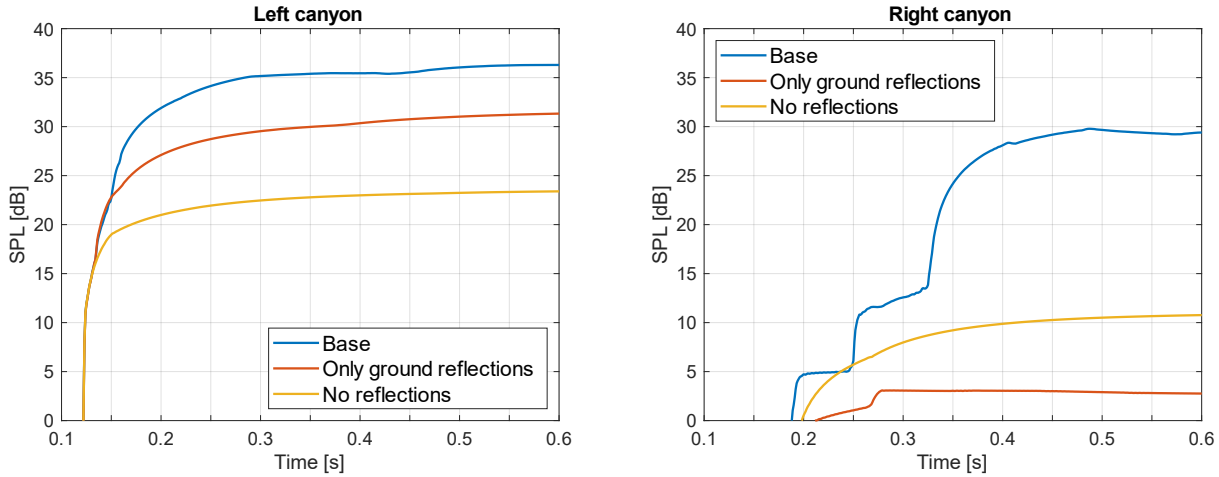

Figure 5.8. Comparison of transient SPL at the bottom-centre of the street canyons.

5.2. NoiseModelling

With NoiseModelling the goal of simulations has been to prepare a set up that could be validated in the future when members of national project MODERA, focused on the study of noise propagation from UAVs in urban areas, take experimental measurements. Instead of considering different case scenarios, the dependency of results on the order of reflections and diffraction on horizontal edges has been put to the test.

When computing a noise map from a point source in NoiseModelling, there are multitude of parameters that can be specified. Among these, air temperature has been set to 20 °C, wall absorption coefficient to 0.9 (almost completely reflective, based on the studies reviewed at Section 3[12], [13], [14], [25], [33], [35]) and maximum source-receiver distance to 800 m. Furthermore, for the base case of study, order of reflections is 3, and diffractions on horizontal edges are computed. The results are shown in Figure 5.9. All results are below 25 dB, which is close to what was seen in the simulation of openCFS with no reflections (see Figure 5.8.). It cannot be claimed if this is due to the problem concerning a much more open domain, because of the different calculation methods or just a coincidence. On another note, it is interesting to see that noise is recorded also behind buildings, proving that reflections and/or diffractions are being considered.

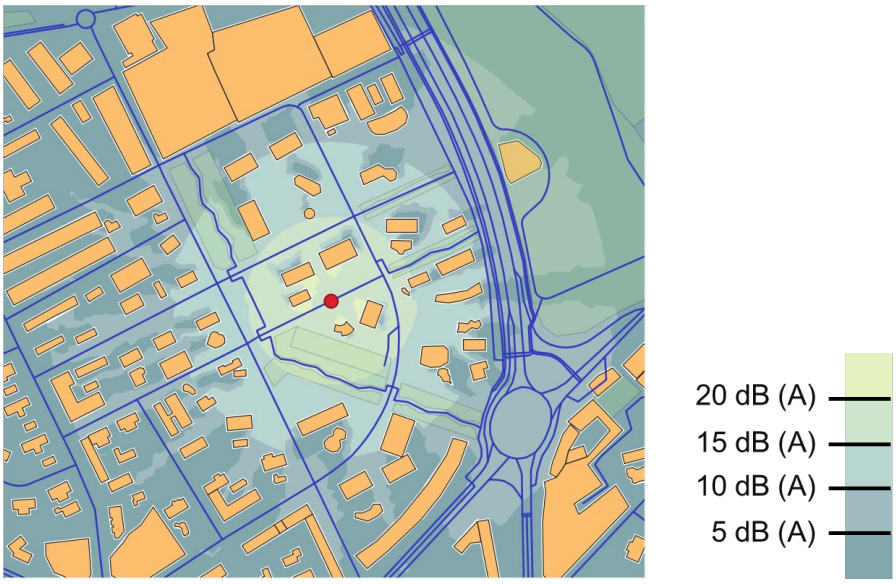

Figure 5.9. Noise map produced with diffraction and reflections of order 3.

After computing a satisfactory first noise map, it has been deemed of interest to study how much the solution changes if order of reflections is reduced. In Figure 5.10. results with order 1 and 2 can be seen. Both are almost equal, only appearing a slight increase of noise in the region closest to the UAV, better seen in Figure 5.10., and the noise map produce with order two is indistinguishable from the one produced with order three (see Figure 5.9.).

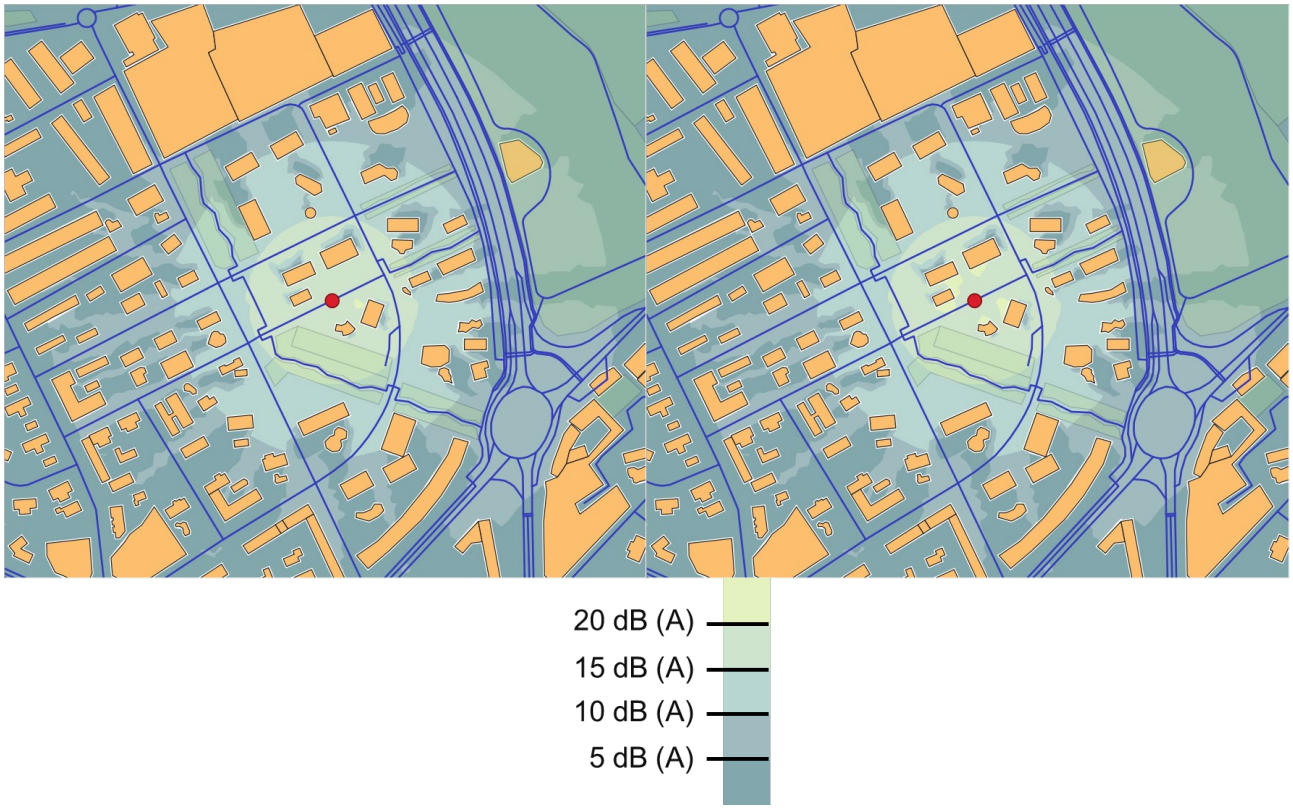

Figure 5.10. Noise maps produced with diffraction, and with reflections of order 1 (left) and 2 (right).

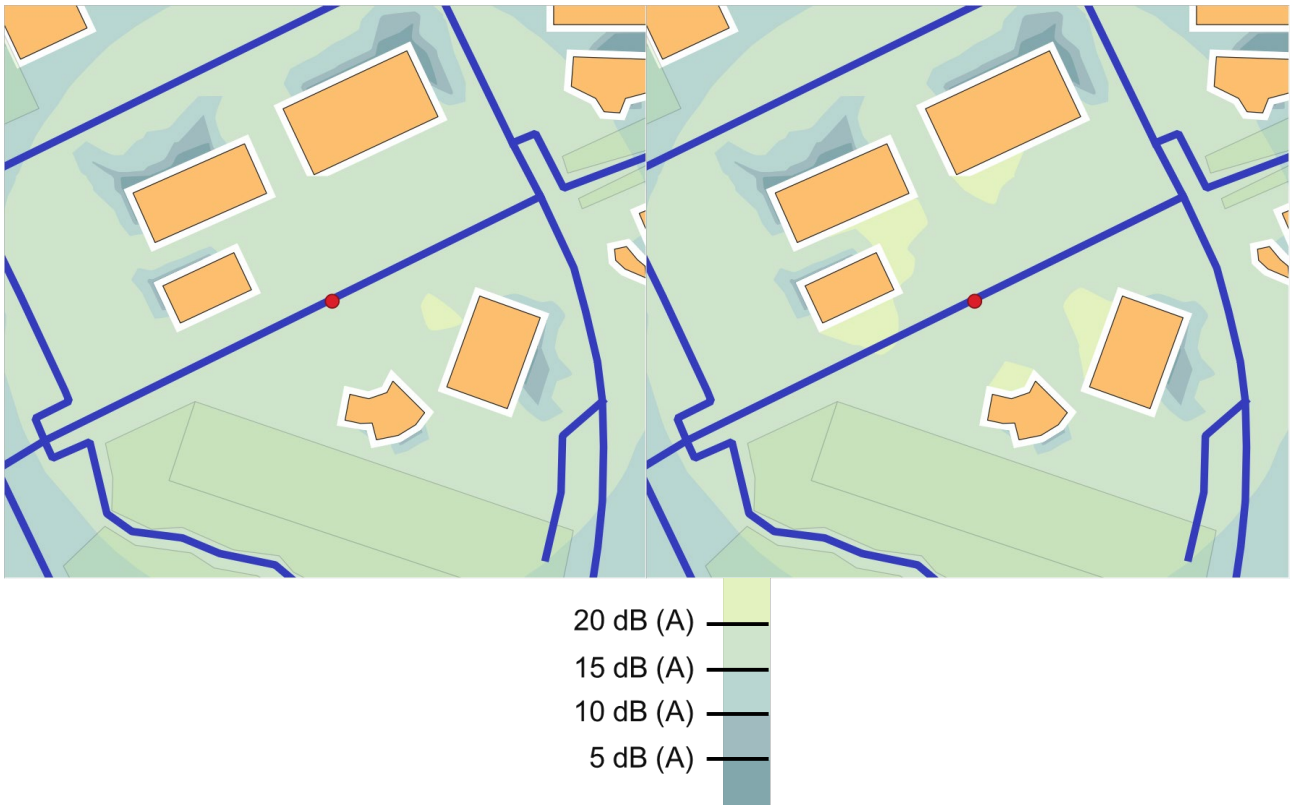

Figure 5.11. Close-up of the noise maps produced with diffraction, and with reflections of order 1 (left) and 2 (right).

As reflections of order 1 and 2 are that similar, next step has been to remove diffractions completely. When first examining Figure 5.12. it may look like no difference has been produced. On closer inspection, (see Figure 5.13), the 'noise shade' produced by buildings is slightly larger when diffractions are not considered. The effect being difficult to perceive coincides with what was revealed by the openCFS simulations: the diffracted wavefronts have much less power than direct impinging or even reflected waves.

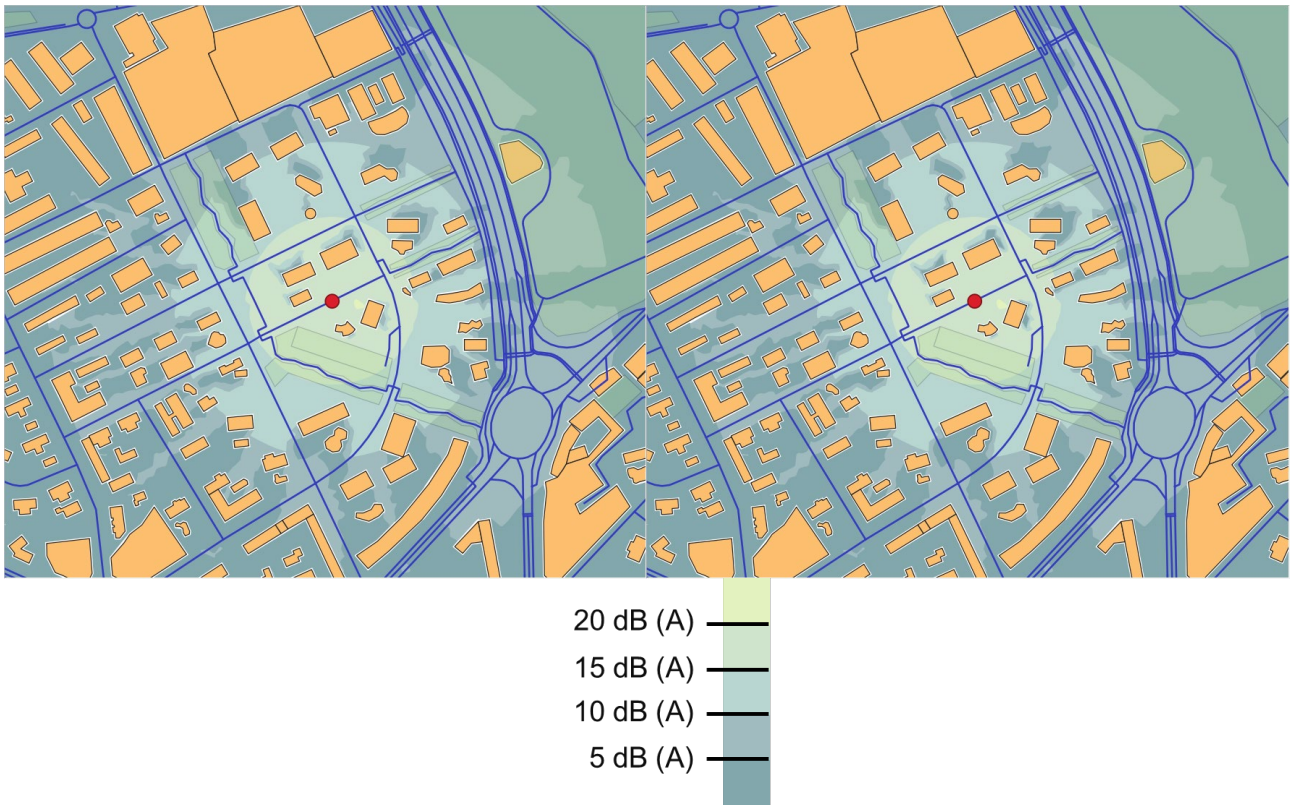

Figure 5.12. Noise maps produced by first order reflections and with (left) and without (right) modelling diffraction.

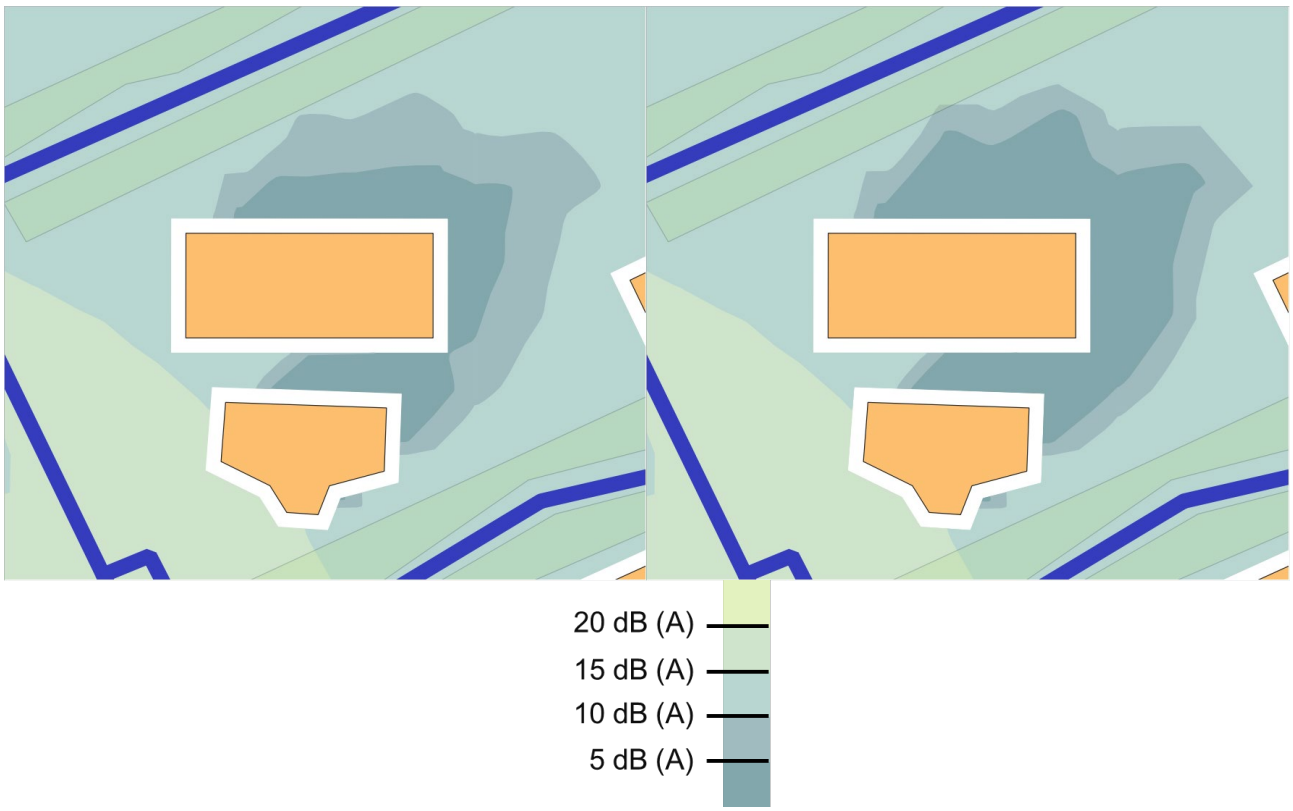

Figure 5.13. Detail of the noise maps produced by first order reflections and with (left) and without (right) modelling diffraction.

The last experiment was to check what would happen if the maximum source-reflection distance was change from 50 m to 800 m (same value as maximum source-receiver distance). Reflections were changed back to third order and diffractions turned on. Yet again, results are almost identical (see Figure 5.14.) and only on close inspection differences can be found (see Figure 5.15).

After performing multiple tests, it seems that, for a single source point in an open domain, default parameters (first order reflections and no diffractions) provide results almost as accurate as those achieved when using higher order reflections and diffractions. However, this can be said for this specific scenario and no extra conclusions should be drawn. As for the results themselves, they seem plausible, but until there is a way to validate the results, it only serves as a rough estimate.

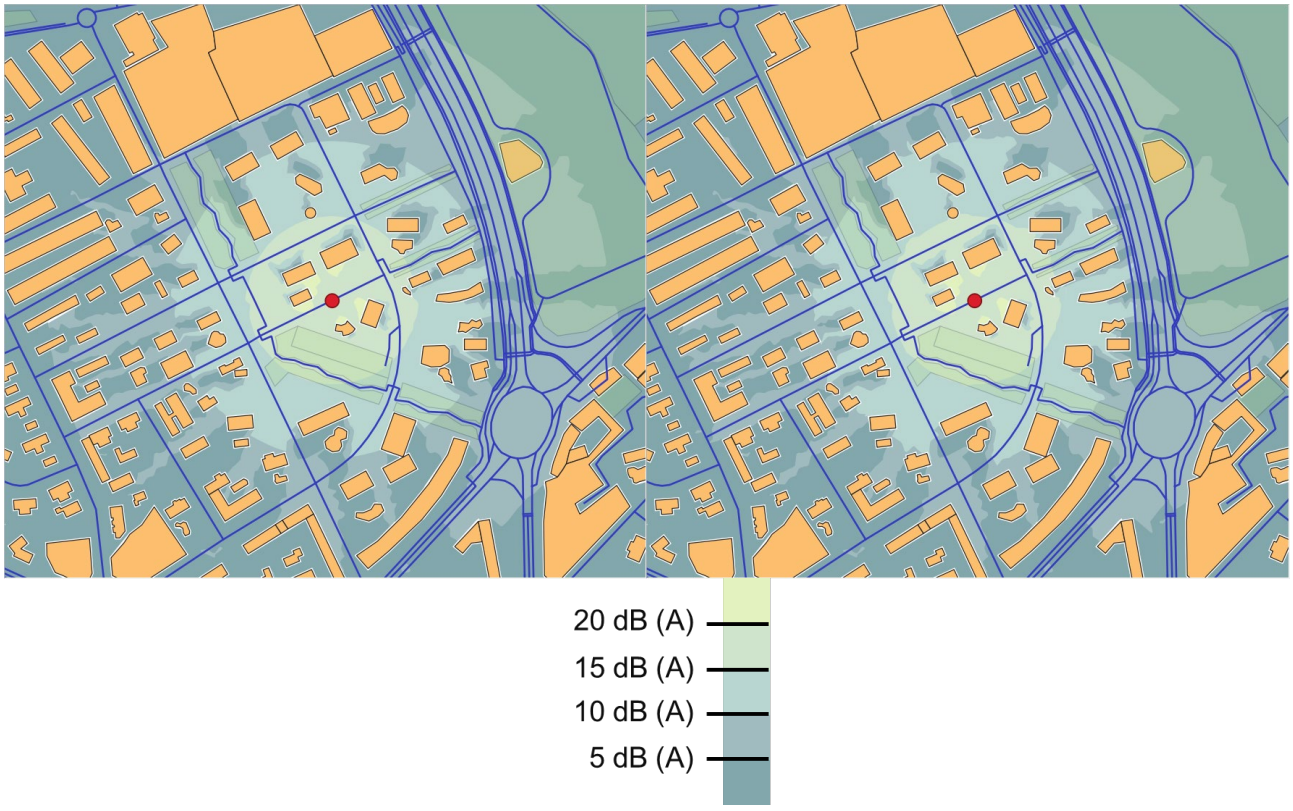

Figure 5.14. Comparison of noise maps produced when the maximum source-reflection distance is set to 50 (left) and 800 m (right).

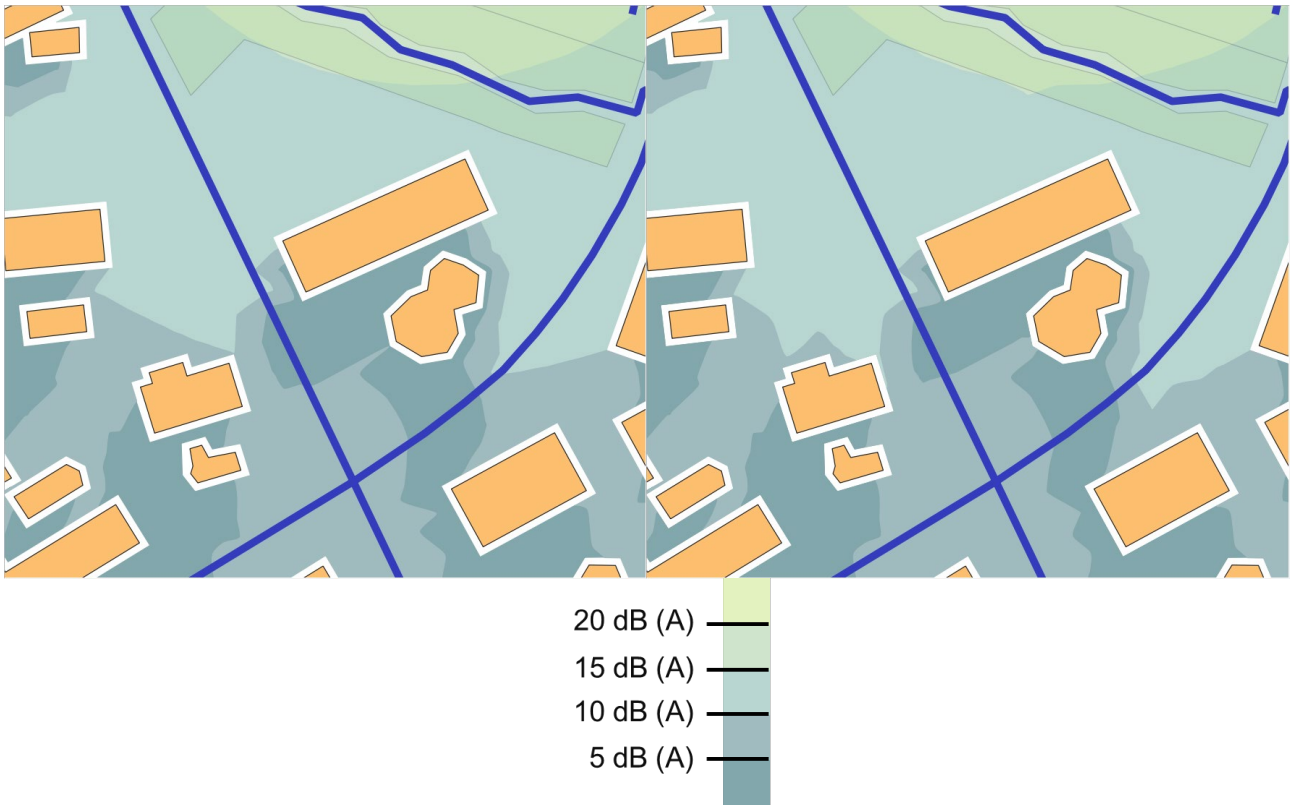

Figure 5.15. Close-up of the comparison of noise maps produced when the maximum source-reflection distance is set to 50 (left) and 800 m (right).

6. Conclusions

The field of sound propagation is currently becoming very active, as UAVs and UAMs are predicted to proliferate in urban spaces in the near future. Due to health and safety concerns, it is necessary to be able to assess beforehand the impact that activities such as parcel delivery or personal travel in UAMs could have in the soundscape. Because of these reasons, this work has been conceived as a means to gather knowledge on the field and find resources to make possible future research.

In this thesis, an in-depth analysis of the field of noise propagation modelling has been done. A description of the theoretical background needed to understand research, as well as a review of the current state of the art has been provided. Furthermore, a comparison of available software to perform numerical simulations of noise propagation has been done. Two different programs were deemed appropriate for simulations, openCFS and NoiseModelling, and as such, their capabilities have been put to the test.

OpenCFS allows to perform precise transient and harmonic simulations using FEM. Both harmonic and transient simulations of a 2D domain were performed. The problem studied had a hovering UAV modelled as a directional source over two street canyons. Simulations proved the capabilities of wave-based methods to model accurately reflections and diffractions.

NoiseModelling is a noise mapping software, and as such, allows to compute big 3D domains in a timely manner, using geometrical acoustics as described by the CNOSSOS-EU methods. Simulations of the same UAV hovering over the Spanish city of Benidorm were performed, varying the order of reflections and deactivating diffractions to see the impact on the results. The city of Benidorm was chosen as national project MODERA will be performing flight test, whose data could be used to validate simulations.

6.1. Future work

After the finalisation of this project multiple routes can be taken. On the one hand, continuing using the proposed software to perform other noise propagation simulations. OpenCFS can be used in clusters to compute more complex problems that do not have to be exclusively acoustic, as it allows to solve problems with mechanical-acoustic coupling, and aeroacoustics.

On the other hand, an in-house numerical solver could be developed based on what was learn the state of the art. If this were the case, the most promising alternatives are FDTD parallelized in GPUs for maximum accuracy simulations, GBT with the inclusion of diffracted beams or ARD for homogeneous domains. An alternative is to couple a geometrical acoustic solver, for higher frequencies, with a wave-based method for lower frequencies, to maximize both efficiency and accuracy.

References

[1] A. W. Sudbury and E. B. Hutchinson, 'A Cost Analysis of Amazon Prime Air (Drone Delivery)', *Journal for Economic Educators*, vol. 16, no. 1, pp. 1–12, Jul. 2016, [Online]. Available: https://ideas.repec.org/a/mts/jrnlee/v16y2016i1p1-12.html

[2] J. P. Aurambout, K. Gkoumas, and B. Ciuffo, 'Last mile delivery by drones: an estimation of viable market potential and access to citizens across European cities', *European Transport Research Review*, vol. 11, no. 1, Dec. 2019, doi: 10.1186/s12544-019-0368-2.

[3] C. C. Murray and A. G. Chu, 'The flying sidekick traveling salesman problem: Optimization of drone-assisted parcel delivery', *Transp Res Part C Emerg Technol*, vol. 54, pp. 86–109, May 2015, doi: 10.1016/j.trc.2015.03.005.

[4] P. Yedavalli *et al.*, 'An Assessment of Public Perception of Urban Air Mobility (UAM)', [Online]. Available: https://api.semanticscholar.org/CorpusID:208253593

[5] M. Nentwich and D. M. Horváth, 'Vision Lieferdrohnen', *TATuP - Zeitschrift für Technikfolgenabschätzung in Theorie und Praxis*, vol. 27, no. 2, pp. 46–52, Jul. 2018, doi: 10.14512/tatup.27.2.46.

[6] H. Eißfeldt *et al.*, 'The acceptance of civil drones in Germany', *CEAS Aeronaut J*, vol. 11, no. 3, pp. 665–676, Sep. 2020, doi: 10.1007/s13272-020-00447-w.

[7] M. Hornikx, 'Ten questions concerning computational urban acoustics', *Build Environ*, vol. 106, pp. 409–421, Sep. 2016, doi: 10.1016/j.buildenv.2016.06.028.

[8] A. Christian and R. Cabell, 'Initial Investigation into the Psychoacoustic Properties of Small Unmanned Aerial System Noise', in *23rd AIAA/CEAS Aeroacoustics Conference*, Jul. 2017. doi: 10.2514/6.2017-4051.

[9] A. J. Torija, Z. Li, and R. H. Self, 'Effects of a hovering unmanned aerial vehicle on urban soundscapes perception', *Transp Res D Transp Environ*, vol. 78, Jan. 2020, doi: 10.1016/j.trd.2019.11.024.

[10] V. E. Ostachev and D. K. Wilson, *Acoustics in Moving Inhomogeneous Media*, Second Edition. 2016.

[11] N. Raghuvanshi, R. Narain, and M. C. Lin, 'Efficient and accurate sound propagation using adaptive rectangular decomposition', in *IEEE Transactions on Visualization and Computer Graphics*, Sep. 2009, pp. 789–801. doi: 10.1109/TVCG.2009.28.

[12] T. Van Renterghem, E. Salomons, and D. Botteldooren, 'Parameter study of sound propagation between city canyons with a coupled FDTD-PE model', *Applied Acoustics*, vol. 67, no. 6, pp. 487–510, Jun. 2006, doi: 10.1016/j.apacoust.2005.09.006.

[13] H. Montanaro, J. Knöpfel, K. Heutschi, and R. Pieren, 'Parallelized FDTD simulations to improve engineering models of urban road traffic noise', in *24th international congress on acoustics. ICA 2022*, Acoustical Society of Korea, 2022.

[14] M. Parker, S. Ketcham, and H. Cudney, 'Acoustic Wave Propagation in Urban Environments', in *2007 DoD High Performance Computing Modernization Program Users Group Conference*, Jun. 2007, pp. 233–237. doi: 10.1109/HPCMP-UGC.2007.7.

[15] V. E. Ostashev, D. K. Wilson, L. Liu, D. F. Aldridge, N. P. Symons, and D. Marlin, 'Equations for finite-difference, time-domain simulation of sound propagation in moving inhomogeneous media and numerical implementation', *J Acoust Soc Am*, vol. 117, no. 2, pp. 503–517, Feb. 2005, doi: 10.1121/1.1841531.

[16] Y. Miki, 'Acoustical properties of porous materials-Modifications of Delany-Bazley models-', *Journal of the Acoustical Society of Japan (E)*, vol. 11, no. 1, pp. 19–24, 1990, doi: 10.1250/ast.11.19.

[17] C. Dreier and M. Vorlaender, 'Vehicle pass-by noise auralization in a virtual urban environment', Jul. 2022.

[18] J.-P. Berenger, 'A perfectly matched layer for the absorption of electromagnetic waves', *J Comput Phys*, vol. 114, no. 2, pp. 185–200, 1994, doi: https://doi.org/10.1006/jcph.1994.1159.

[19] X. Yuan, D. Borup, J. W. Wiskin, M. Berggren, R. Eidens, and S. A. Johnson, 'Formulation and validation of Berenger's PML absorbing boundary for the FDTD simulation of acoustic scattering', *IEEE Trans Ultrason Ferroelectr Freq Control*, vol. 44, no. 4, pp. 816–822, 1997, doi: 10.1109/58.655197.

[20] F. L. Teixeira and W. C. Chew, 'Complex space approach to perfectly matched layers: a review and some new developments', *International Journal of Numerical Mod-*

elling: Electronic Networks, Devices and Fields, vol. 13, no. 5, pp. 441–455, Sep. 2000, doi: 10.1002/1099-1204(200009/10)13:5<441::AID-JNM376>3.0.CO;2-J.

[21] A. Bermúdez, L. Hervella-Nieto, A. Prieto, and R. Rodríguez, 'An optimal perfectly matched layer with unbounded absorbing function for time-harmonic acoustic scattering problems', *J Comput Phys*, vol. 223, no. 2, pp. 469–488, May 2007, doi: 10.1016/j.jcp.2006.09.018.

[22] K. K. Iu and K. M. Li, 'The propagation of sound in narrow street canyons', *J Acoust Soc Am*, vol. 112, no. 2, pp. 537–550, Aug. 2002, doi: 10.1121/1.1492821.

[23] A. D. Pierce, *Acoustics: an introduction to its physical principles and applications*, 3rd edition. Springer, 2019.

[24] M. B. Porter and H. P. Bucker, 'Gaussian beam tracing for computing ocean acoustic fields', *J Acoust Soc Am*, vol. 82, no. 4, pp. 1349–1359, Oct. 1987, doi: 10.1121/1.395269.

[25] F. Yunus, D. Casalino, F. Avallone, and D. Ragni, 'Urban air mobility noise prediction in a 3D environment using Gaussian beam tracing', in *DICUAM 2022*, Jul. 2022.

[26] M. Popov and I. Pšenčík, 'Computation of Ray Amplitudes in Inhomogeneous Media with Curved Interfaces', *Studia Geophysica et Geodaetica*, vol. 46, pp. 1–11, Jul. 2002, doi: 10.1023/A:1024844225542.

[27] M. Mikhailovich. Popov and Universidade Federal da Bahia. Instituto de Geociências., *Ray theory and gaussian beam method for geophysicists*. EDUFBA, 2002.

[28] M. R. Schroeder, 'The "'Schroeder frequency'" revisited', *J Acoust Soc Am*, vol. 99, no. 5, pp. 3240–3241, May 1996, doi: 10.1121/1.414868.

[29] Stylianos. Kephalopoulos, Marco. Paviotti, Fabienne. Anfosso-Lédée, and Institute for Health and Consumer Protection., *Common noise assessment methods in Europe (CNOSSOS-EU) : to be used by the EU Member States for strategic noise mapping following adoption as specified in the Environmental Noise Directive 2002/49/EC.* OPEU, 2012.

[30] R. Mehra, N. Raghuvanshi, L. Savioja, M. C. Lin, and D. Manocha, 'An efficient GPU-based time domain solver for the acoustic wave equation', *Applied Acoustics*, vol. 73, no. 2, pp. 83–94, Feb. 2012, doi: 10.1016/j.apacoust.2011.05.012.

[31] L. Antani, A. Chandak, M. Wilkinson, A. A. Bassuet, and D. Manocha, 'Validation of adaptive rectangular decomposition for three-dimensional wave-based acoustic simulation in architectural models', in *Proceedings of Meetings on Acoustics*, 2013. doi: 10.1121/1.4800221.

[32] R. Mehra, N. Raghuvanshi, A. Chandak, D. G. Albert, D. Keith Wilson, and D. Manocha, 'Acoustic pulse propagation in an urban environment using a three-dimensional numerical simulation', *J Acoust Soc Am*, vol. 135, no. 6, pp. 3231–3242, Jun. 2014, doi: 10.1121/1.4874495.

[33] D. Casalino, M. Barbarino, and A. Visingardi, 'Simulation of helicopter community noise in complex urban geometry', *AIAA Journal*, vol. 49, no. 8, pp. 1614–1624, Aug. 2011, doi: 10.2514/1.J050774.

[34] M. Barbarino, F. Petrosino, and A. Visingardi, 'A high-fidelity aeroacoustic simulation of a VTOL aircraft in an urban air mobility scenario', *Aerosp Sci Technol*, vol. 125, Jun. 2022, doi: 10.1016/j.ast.2021.107104.

[35] Q. Tan *et al.*, 'Virtual flight simulation of delivery drone noise in the urban residential community', *Transp Res D Transp Environ*, vol. 118, May 2023, doi: 10.1016/j.trd.2023.103686.

[36] J. Kennedy, S. Garruccio, and K. Cussen, 'Modelling and mitigation of drone noise', in *Vibroengineering Procedia*, EXTRICA, May 2021, pp. 60–65. doi: 10.21595/vp.2021.21988.

[37] K. Cussen, S. Garruccio, and J. Kennedy, 'UAV Noise Emission—A Combined Experimental and Numerical Assessment', *Acoustics*, vol. 4, no. 2, pp. 297–312, Jun. 2022, doi: 10.3390/acoustics4020018.

[38] S. Kephalopoulos, M. Paviotti, F. Anfosso-Lédée, D. Van Maercke, S. Shilton, and N. Jones, 'Advances in the development of common noise assessment methods in Europe: The CNOSSOS-EU framework for strategic environmental noise mapping', *Science of the Total Environment*, vol. 482–483, no. 1, pp. 400–410, Jun. 2014, doi: 10.1016/j.scitotenv.2014.02.031.

[39] M. Kaltenbacher *et al.*, 'openCFS', CFS-2024S-Linux. [Online]. Available: https://opencfs.org

[40] CNRS and Université Gustave Eiffel, 'NoiseModelling'.

[41] J. Serrano, J. García-Tíscar, P. Quintero, and F. Ramírez, 'Numerical and Experimental Evaluation of Noise and Performance in UAV Propellers', in *ASME Turbo Expo 2023: Turbomachinery Technical Conference and Exposition*, Jul. 2023. doi: 10.1115/GT2023-102389.

[42] B. Hamilton, 'PFFDTD Software', 2021.

[43] L. Van Harten, M. Hornikx, and T. Krijnen, 'openPSTD'.

[44] M. Hornikx, T. Krijnen, and L. van Harten, 'openPSTD: The open source pseudospectral time-domain method for acoustic propagation', *Comput Phys Commun*, vol. 203, pp. 298–308, 2016, doi: https://doi.org/10.1016/j.cpc.2016.02.029.

[45] S. Schoder and K. Roppert, *openCFS: Open Source Finite Element Software for Coupled Field Simulation -- Part Acoustics*. 2022. doi: 10.48550/arXiv.2207.04443.

[46] Université Gustave Eiffel - Environmental Acoustics Research Unit (UMRAE), 'i-Simpa'.

[47] J. Picaut and N. FORTIN, 'SPPS, a particle-tracing numerical code for indoor and outdoor sound propagation prediction', Apr. 2012.

[48] EDF R&D, 'Code_TYMPAN'.

[49] C. Geuzaine and J.-F. Remacle, 'Gmsh'.

[50] OpenStreetMap Foundation, 'OpenStreetMap'. [Online]. Available: https://www.openstreetmap.org

[51] W. Schneider, 'BBBike.org'. [Online]. Available: https://extract.bbbike.org/

[52] QGIS Foundation, 'QGIS'.

Appendix A: Project's Budget

Hereunder an estimation of the monetary costs of the work carried out during the thesis is presented. Both costs due to people involved in the project and costs proceeding from the use of material resources have been considered. A list of tasks performed during the realisation of the project is listed below, as well as a breakdown of material resources that were required.

A.1. Tasks performed by personnel involved

This project can be split into a research part and another one of simulations:

1. **Research:**
    a. Study of the state of the art: first step in the project was to learn about the field of sound propagation models. Extensive documentation was gathered and inspected to gain an understanding of the underlying physics and the characteristics of each method of calculation.
    b. Search of available software: next, multiple software alternatives were reviewed. Simple simulations and tutorials were carried out with software that ended up being discarded.
2. **Simulations**:
    a. Familiarisation with the software: not only the software used for simulations themselves have to be learnt, but also compatible software for pre- and post-processing of results.
    b. Definition of the simulations and pre-processing: once the capabilities and possibilities of the software were known, two base simulations were defined (one for openCFS and another one for NoiseModelling). Variations of this base cases were also thought out to compare results.
    c. Simulations and post-processing: simulations were then launched. Afterwards, results had to be post-processed to obtain relevant and useful information from the simulations.
3. **Drafting of this thesis**: the thesis had to be written and reviewed. The project's defence also had to be prepared.

A.2. Resources employed

Resources employed include personal involved, software and equipment. Table A.1. contains all resources used during the elaboration of the project.

Personnel	Software	Equipment
PhD Researcher	openCFS	Personal laptop
PhD candidate	NoiseModelling	Rigel
Engineer	Gmsh	
	QGIS	
	MATLAB	
	ParaView	
	Microsoft Word	

Table A.1. Resources employed in the project's elaboration.

A.3. Costs

A.3.1. Personnel

People involved in the project were a PhD researcher, a PhD candidate and an engineer (the author of the work). Gross annual salaries have been used to obtain cost per hour:

- **PhD researcher hired as a professor:** tutor of the project. Gross annual salary of 42 000 €, hence 23.10 €/h.
- **PhD candidate:** cotutor of the project. Gross annual salary of 30 000 €, hence 16.48 €/h.
- **Engineer:** author of the project. Gross annual salary of 21 000 €, hence 11.54 €/h.

A breakdown of hours of work in each of the project's tasks can be seen in Table A.2., in which the gross monetary cost of the personnel is calculated.

		Hours	Salary	Cost
PhD researcher	Task 1.a	15	23.10 €/h	346.50 €
	Task 1.b	15		346.50 €
	Task 2.a	0		0.00 €
	Task 2.b	0		0.00 €
	Task2.c	0		0.00 €
	Task 3	10		231.00 €
PhD candidate	Task 1.a	15	16.48 €/h	247.20 €
	Task 1.b	15		247.20 €
	Task 2.a	10		164.80 €
	Task 2.b	20		329.60 €
	Task2.c	10		164.80 €
	Task 3	15		247.20 €
Engineer	Task 1.a	60	11.54 €/h	692.40 €
	Task 1.b	50		577.00 €
	Task 2.a	55		634.70 €
	Task 2.b	40		461.60 €
	Task2.c	20		230.80 €
	Task 3	70		807.80 €
		TOTAL		5729.10 €

Table A.2. Gross personnel costs.

A.3.2. Software

Most of the software that has been used during this thesis are open-source, hence they do not have any cost. The exceptions are MATLAB and Microsoft Word. The costs associated with the licenses of these software are included in Table A.3.:

Software	Cost
MATLAB	860.00 €
Microsoft Office	69.00 €
TOTAL	929.00 €

Table A.3. Software costs.

A.3.3. Equipment

Regarding equipment, on the one hand, the amortisation period of a computer is usually established at 5 years, hence university equipment does not contribute to total costs. On the other hand, a personal laptop, which had a cost of 983 €, was acquired in September 2020, hence it was only 3 years old at the start of this project. The 40% of its cost, 393.20 €, has, therefore, being included in the budget.

Furthermore, some calculations were performed on a node of the internal cluster of the UPV, Rigel, which has a cost of 0.01 €/(h core). Taking into account that all 48 cores of the node were used and that, between the simulations that were not correctly defined and the ones that have been included in the thesis, the node has been running for 100 h, the associated cost is 48 €.

A.3.4. Total costs

Considering all expenses described above, the total cost of the project is calculated. In Table A.4. the gross total cost of the project is shown. Finally, in Table A.5. the final cost if shown, accounting for indirect expenses, industrial profit an IVA.

Concept	Cost
Personnel	5729.10 €
Software	929.00 €
Equipment	441.20 €
GROSS TOTAL	7099.30 €

Table A.4. Gross total cost of the project.

Concept		Cost
Gross cost		7099.30 €
Indirect expenses	25%	1774.83 €
Industrial profit	6%	425.96 €
IVA	21%	1490.85 €
	TOTAL COST	10790.94 €

Table A.5. Final cost of the whole project.

The total cost of the project is:

 # TEN THOUSAND SEVEN HUNDRED NINETY EUROS AND NINETY-FOUR CENTS#

Appendix B: Bid specifications

While working on any project, the safety and health of the engineer must be ensured at the place of work. Rules are established by regulatory institutions to this end. Specifically, in Spain, Real Decreto 486/1997, from the 14th of April, lays down minimum safety and health requirements for workplaces.

For the purposes of this regulation, it will be considered that a workplace is any area, built-up or not, in which workers are required to remain or to which they may have access by reason of their work. Hygiene services and rest areas, first aid facilities and canteens are considered to be included in this definition, even if they are not directly integrated in the workplace.

In this case, workplaces include the Clean Mobility & Thermofluids (CMT) research centre and the homeplace of the author of this work. Both are required to meet the same regulations.

B.1. Workplace specifications

B.1.1. General safety specifications

It must be ensured that the workplace has adequate infrastructure that guarantees safety. Minimum requirements to the dimensions of the workplace are roofs at least 3 m high (though it may be reduced to 2.5 m in offices), and a surface and volume of 2 m^2 and 10 m^3 per worker.

A good ventilation is also a basic necessity for the well-being and productivity of workers. The ventilation system must be adequate to the number of people inside the building, as well as other relevant factors.

Basic safety protocols include evacuation procedures: there must be enough exits for all workers to evacuate as fast as possible, and all emergency exits must be opened outwards and remain opened to ease the evacuation process. No obstacles can block these exits at any point. Additionally, these doors must not be sliding or turning doors, as they can hinder fast and safe evacuation under stress or panic conditions.

Firefighting tools must comply with legislation. Fire extinguishers, smoke detectors, automatic sprinklers, etc. have to be present in all floors in enough number, according to the number of workers and dimensions of the workplace.

On another note, the workplace must be accessible to disabled people, making sure that stairs, bathrooms and corridors are correctly adapted.

B.1.2. Order, cleanliness and maintenance

All working areas, including offices, meeting rooms, common areas and sanitary facilities, must be cleaned regularly and thoroughly. This includes vacuuming, sweeping and scrubbing of floors, cleaning of surfaces, furniture and equipment, and the disposal of waste. Besides, organization and order must be adequate to avoid obstructions. Also, cleaning procedures must not put workers at risk.

Special care must be taken when cleaning sanitary installations. Frequent disinfection of surfaces is needed, and supplies of products like soap or paper ensured.

The facilities must be subjected to maintenance regularly, so that safety conditions can be guaranteed.

B.1.3. Ambient specifications

The temperature of premises where sedentary work is carried out in offices or similar premises shall be between 17 and 27 °C. Furthermore, the relative humidity must be between 30 and 70%. Also, workers must not be exposed frequently or continuously to air currents exceeding 0.25 m/s in not hot environments or 0.5 m/s in hot environments, not including currents produced by air conditioning, which cannot exceed 0.25 m/s in any case in workplaces where sedentary works are carried out.

Regarding air renovation, a minimum of at least 30 $m^3/(h \cdot worker)$ of clean air is required in sedentary works in environments not hot neither polluted by tobacco smoke, and 50 $m^3/(h \cdot worker)$ in all the other cases.

B.1.4. Workplace lighting

Lighting of each area of the workplace has to be adapted to the activities performed in it. If possible, workplaces will have natural lighting complemented with artificial lighting when the former is not enough. In areas where tasks with a moderate visual demand are carried out, a minimum level of 200 lux is required. Lighting also has to be as uniformly distributed as possible, avoiding abrupt variations of luminance within and between the area of operation and its surroundings.

Direct sun glare or glare produced by any artificial source of light must be avoided. No light sources can be placed without protection in the worker's field of view.

B.1.5. Restrooms and resting places

Drinkable water must be accessible and provided in enough quantities. Workplaces must have nearby restrooms with sinks and mirrors, soap and a drying mechanism that ensures hygiene. However, resting places are not required for office workers, provided that the office provides enough rest amenities during breaks.

B.1.6. First aid equipment and facilities

Workplaces must have first aid material in case an accident takes place. Characteristics and amount of material must be adequate to the number of workers and the risks associated with the activities carried out. The material must be placed and distributed so that it can be easily accessed by all workers. Every workplace shall have at least a portable first-aid kit containing authorised disinfectants and antiseptics, sterile gauze, hydrophilic cotton, bandages, adhesive plasters, adhesive dressings, scissors, tweezers and disposable gloves. In cases where there are more than 50 workers, an area must be designated to first aid needs, with a first aid kit and a stretcher. The first aid material and first aid areas must be clearly indicated.

B.2. Technical specifications

To carry out the simulations seen in this work, both hardware and software resources have been necessary. As the possibility of elaborating this project is tied to these, they also are part of the required specifications.

B.2.1. Hardware specifications

Most of the work has been carried out in a personal laptop. Specifications of this laptop can be seen in Table B.1.:

Model	HP Pavillion
Processor	Intel Core i7-10750H CPU @ 2.60 GHz 2.59 GHz (6 cores, 12 threads)
RAM	16.0 GB (15.8 GB usable)
Storage	Solid State Disk (SSD) with 512 GB
GPU	NVIDIA GeForce RTX 2060 with Max-Q Design

Table B.1. Specifications of personal laptop.

Additionally, time-domain FEM simulations were run on a single node of cluster Rigel from the UPV. The node has an Intel® Xeon® Gold 6248R processor with 48 cores, and a RAM memory of 185 GB.

B.2.2. Software specifications

A list of software that has been used during the elaboration of this work is given below:

— **openCFS:** version CFS-2024S-Linux has been used. It is a free open-source software.
— **NoiseModelling:** version 4.0.5 has been employed during the realisation of this work. It is a free open-source software as well.
— **Gmsh:** it is an open-source mesher that has been used for pre-processing of the openCFS simulations. Version employed was 4.11.1-Windows64.
— **ParaView:** open-source software used to post-process simulation results, extract data and obtain images. Version 5.12.1, which includes the CFSReader plugin, has been used to post-process openCFS simulations.
— **QGIS:** desktop 3.36.2 version has been employed for both pre- and post-processing of NoiseModelling simulations. It is also a free open-source software.
— **MATLAB:** commercial programming software. Version R2022b has been used to access simulation data, and to create directivity files.
— **Microsoft Word (Office 365):** the entirety of this work has been written in Microsoft Word, program belonging to the subscription service Office 365.

Appendix C: Relationship of the thesis with the Sustainable Development Goals

Table C.1. indicates to which extent this thesis is related to the Sustainable Development Goals (SDG) of the 2030 Agenda:

Sustainable Development Goals	High	Medium	Low	Not applicable
SDG 1. **No poverty.**				X
SDG 2. **Zero hunger.**				X
SDG 3. **Good health and well-being.**	X			
SDG 4. **Quality education.**				X
SDG 5. **Gender equality.**				X
SDG 6. **Clean water and sanitation.**				X
SDG 7. **Affordable and clean energy.**				X
SDG 8. **Decent work and economic growth.**				X
SDG 9. **Industry, innovation and infrastructure.**			X	
SDG 10. **Reduced inequalities.**				X
SDG 11. **Sustainable cities and communities.**		X		
SDG 12. **Responsible consumption and production.**				X
SDG 13. **Climate action.**				X
SDG 14. **Life below water.**				X
SDG 15. **Life on land.**	X			
SDG 16. **Peace, justice and strong institutions.**				X
SDG 17. **Partnerships for the goals.**				X

Table C.1. Relationship of the thesis with the Sustainable Development Goals.

How the work is related to the SDGs indicated in Table C.1. is briefly explained below:

— **SDG 3. Good health and well-being:** this thesis is focused on the assessment of available tools to study sound propagation in urban environments. The apparition of new noise sources is concerning, as high noise levels can

produce high levels of stress and loss of focus. These affections can favour the apparition of other serious pathologies. It is therefore important to prevent noise pollution anticipating the effects that UAVs and UAMs could bring to the soundscape.

— **SDG 9. Industry, innovation and infrastructure:** sound propagating simulations are an active field of research that can be applied also to assessing noise levels in industry plants and to realistic virtual environments.

— **SDG 11. Sustainable cities and communities:** electric UAVs and UAMs could replace in the future polluting alternatives that rely on fossil fuels. On the other hand, noise is another kind of pollution that should be kept to a minimum in sustainable cities and communities.

— **SDG 15. Life on land:** noise pollution is an even bigger concern to animals than to humans. High levels of noise can confuse animals, making them to put themselves in danger, and also simply altered their biological rhythms.